

# POPULATIONS IN SPATIAL EQUILIBRIUM\*

Matthew Easton                    Patrick W. Farrell  
Cornerstone Research              Columbia University

This Version: October 2025

[Click here for latest version](#)

## Abstract

Power law-like distributions for city populations are a distinctive, recurring feature of human settlement patterns. We propose an explanation for this phenomenon that reflects both the qualities of a place (locational fundamentals) and its ability to benefit from trade based on its location (market access). Using random variation in geography to model these two terms within a quantitative spatial model results in both being lognormally distributed and generates a lognormal population distribution, which appears to follow a power law for the most populous locations (i.e., cities). We invert the model on U.S. data and verify our key predictions of lognormal distributions of locational fundamentals and market access.

---

\*Easton: matthew.easton@cornerstone.com. Farrell (corresponding author): pwf2108@columbia.edu. The authors thank Arslan Ali, Nadia Ali, Costas Arkolakis, Pierre-Philippe Combes, Donald R. Davis, Richard A. Davis, Jonathan Dingel, Thibault Fally, Matthieu Gomez, Brian Greaney, Madeline Hansen, Yannis Ioannides, Raphaël Lafrogne-Joussier, Jeffrey Lin, Kosha Modi, Serena Ng, Eshaan Patel, Stephen Redding, Frédéric Robert-Nicoud, Andrés Rodríguez-Clare, Esteban Rossi-Hansberg, Bernard Salanié, Stephan Thies, Lin Tian, Conor Walsh, David Weinstein, Natalie Yang, and seminar and conference participants at Columbia University, the 2024 European Meeting of the Urban Economics Association, the 2024 North American Meeting of the Urban Economics Association, and the 2025 NBER Urban Economics Summer Institute for helpful comments and discussions. Easton acknowledges the Program for Economic Research at Columbia University and the Alliance Doctoral Mobility Grant from Columbia University and Sciences Po for support.

# 1 Introduction

The most remarkable empirical regularity in spatial economics is that the upper tail of the city size distribution appears to follow a power law. Why this regularity arises is a question that quantitative spatial models, which form the basis of modern spatial economics, have thus far failed to answer. While a key feature of these models is their ability to recover the unobserved productivity and amenity values of each location—locational “fundamentals”—which rationalize the observed populations, they do not explain why the underlying locational fundamentals and market access should consistently generate the characteristic city size distribution. By contrast, existing explanations for the appearance of a power law are inconsistent with quantitative spatial models as they allow no role for a location’s characteristics (Brakman et al. 1999; Hsu 2012; Rante et al. 2024), no role for a place’s interactions with other locations (Lee and Li 2013; Behrens and Robert-Nicoud 2015), or no role for either factor to determine a city’s population (Gabaix 1999b). That is, the literature that models the forces shaping cities cannot explain the regularity of the city size distribution, while the literature explaining city size distributions ignores the forces shaping cities.

Our paper shows that random variation in the characteristics of different locations and trade costs can generate the characteristic city size distribution within quantitative spatial models, uniting the canonical models of the spatial economy with the literature on the population distribution. Within the Allen and Arkolakis (2014) quantitative spatial equilibrium framework, we show that the population of each location can be expressed as the product of two terms. One term reflects that location’s own fundamentals. The other term is a trade cost-weighted sum over all locations and represents that location’s market access. First, we incorporate insights from prior literature and model the locational fundamentals within a quantitative spatial model as aggregates of randomly distributed locational attributes that reflect the characteristics of each place. Under general modeling assumptions, the resulting fundamentals will be lognormally distributed by a central limit theorem. Second, we provide a novel proof for the distribution of the market access term, applying a result from Marlow (1967) for central limit theorems over sums of positive random variables. We apply this result to demonstrate that the market access terms will also be lognormally distributed. The population distribution is thus lognormally distributed as the product of two lognormally distributed terms. As a lognormal distribution approximates a power law in the upper tail, our framework naturally generates the characteristic power law-like city size distribution.

We show that an inversion of the model using data for the United States results in log-

normally distributed fundamentals and market access, as predicted by our theory. We then simulate the quantitative spatial model, using parameters drawn from the inversion, to test our framework's robustness and ability to match results in the theoretical and empirical literatures on the city size distribution. We show simulated results in a finite setting and demonstrate that these are consistent with our asymptotic theory. We show that differences in local productivity spillovers, intra-city congestion externalities, and inter-city transportation costs can explain variation in the city size distribution across countries observed in the data. We find that as agglomeration benefits increase the size distribution becomes more unequal, consistent with observed changes to the U.S. city size distribution (Gabaix and Ioannides 2004). Increasing inter-city transportation costs also results in a more unequal city size distribution. This provides a potential explanation for the very large “primate” cities and unequal city size distributions of developing countries, where domestic transportation costs are often much higher than in developed countries (Teravanhorn and Gaël 2009; Atkin and Donaldson 2015).

Our paper touches on several branches of the spatial economics literature. Many theoretical explanations of the city size distribution are based on the similarly striking empirical observation that city growth rates are often unrelated to city population, such as Gabaix (1999a), Gabaix (1999b), Blank and Solomon (2000), Eeckhout (2004), Rossi-Hansberg and Wright (2007), and Córdoba (2008).<sup>1</sup> However, the assumption of random growth is inconsistent with the empirical evidence on the distribution of cities in significant ways. The growth of cities does not appear random in many important cases, particularly following major shocks.<sup>2</sup> Random growth explanations also fail to capture the influence of the characteristics of a place on the attractiveness of producing or residing there, implying that the large populations of New York City, Tokyo, and London are random and unrelated to their advantageous geographies. These theories are also aspatial and do not allow for interactions between different locations to shape settlement patterns, failing to capture the contribution of trade to the scale of the aforementioned global cities.<sup>3</sup>

There are papers within the literature on city size distributions that have accounted for

---

<sup>1</sup>Random growth is often referred to in the literature as Gibrat’s law. The “law” is an application of the central limit theorem to the log of the product of independent shocks, originally formulated to describe the growth of firms (Gibrat 1931).

<sup>2</sup>Notable instances of recovery from shocks are documented in Davis and Weinstein (2002), Brakman et al. (2004), and Davis and Weinstein (2008) following bombings, and in Johnson et al. (2019) following pandemics. Desmet and Rappaport (2017) also document the absence of the random growth phenomenon for cities during the settlement of the American West.

<sup>3</sup>New York City is located on one of the largest natural harbors on Earth and its much greater population relative to Lost Springs, Wyoming—the 2020 population ratio was 8,804,190 to 6—is likely related to New York’s favorable geography and the benefits of its location for trade. Some attributes of landlocked Lost Springs include its low annual precipitation and a coal mine which last operated in the 1930s.

either the role of a place's characteristics or its location in determining its population, but our paper is the first to include these important forces simultaneously. Prior work that does account for the importance of geography or fundamentals, such as Lee and Li (2013) and Behrens and Robert-Nicoud (2015), has lacked trade between locations. In contrast, those papers that account for the importance of trade and market access, such as Brakman et al. (1999), Hsu (2012), and Rante et al. (2024), are models that do not allow for variation in the characteristics of locations. By placing our explanation for the distribution's emergence within a quantitative spatial model, we can include roles for both local characteristics and trade between locations. Further, given the properties of quantitative spatial models, we also demonstrate that population distributions will exhibit random growth in equilibrium in response to increases in the aggregate population level. That is, we demonstrate that random growth is a characteristic of an equilibrium population distribution based on local characteristics of place and trade, rather than being the force that creates the equilibrium population distribution. This provides consistency with the observation of random growth in many contexts that motivated prior models, and its absence following disequilibrating shocks.

By integrating the literature on population distributions with that on quantitative spatial models, we show the conditions under which these models generate the characteristic city size distribution. Models of the spatial economy, beginning with Krugman (1991), Helpman (1998), and Fujita et al. (1999), highlight the roles of space, local spillovers, and the importance of trade between locations in determining population distributions. The spatial literature is now based on quantitative spatial models as developed in Allen and Arkolakis (2014), Redding (2016), and Redding and Rossi-Hansberg (2017). While quantitative spatial models incorporate many of the forces that influence the size of cities, they do not explain the regularity of the population distribution. These models can recover the unobserved qualities of each location, their "fundamentals," which rationalize observed populations. Yet this inversion is possible for any arbitrary vector of "populations," even those with little resemblance to real-world population distributions.<sup>4</sup> We demonstrate how both heterogeneity in the attributes of different places and trade across space will generate lognormal population distributions in equilibrium as a result of random variation in geography. Thus, we show how the models within this literature can be used to provide a deep explanation for why the population tends to be distributed in a particular way within countries. As our result relies solely on variation in geography and applications of a central limit theorem within these models, its simplicity and generality

---

<sup>4</sup>Adão et al. (2023) make a similar point, noting that modern spatial models are saturated with free parameters such that they are always able to exactly match the underlying data.

can explain the consistent observation of this phenomenon in many contexts.

Our framework shows a deep relationship between the heterogeneous attributes of locations, which a broad literature demonstrates are important for local populations, and the shape of the city size distribution. The largest cities around the world tend to be in locations that are good for production, offer quality-of-life benefits to residents, and offer the opportunity to trade with other locations. The literature has found a large role for “first-nature” geographic characteristics in explaining local populations, as in Rappaport and Sachs (2003), Nordhaus (2006), Nunn and Puga (2012), Henderson et al. (2018), Bosker and Buringh (2017), and Alix-Garcia and Sellars (2020). Literature supporting the importance of market access and trade for determining populations and incomes includes Redding and Venables (2004), Redding and Sturm (2008), and Head and Mayer (2011). Further, basing the origin of the population distribution on slow-changing attributes like geography can explain the persistence and resilience of the city size distribution to negative shocks.<sup>5</sup>

The paper proceeds as follows. Section 2 argues that populations are best described by a lognormal distribution and establishes the link between this distribution and the appearance of a power law for cities. Section 3 presents a standard quantitative spatial model and shows that, given the structure of the equilibrium condition, a lognormal population distribution results from both trade across space and random variation in attributes within places. Section 4 provides support for our key modeling assumptions by recovering fundamentals and market access for the U.S. by inverting the model, demonstrating that both are lognormally distributed. We then simulate the model to demonstrate that it captures several results in the empirical literature on city size distributions via simulation. Section 5 concludes.

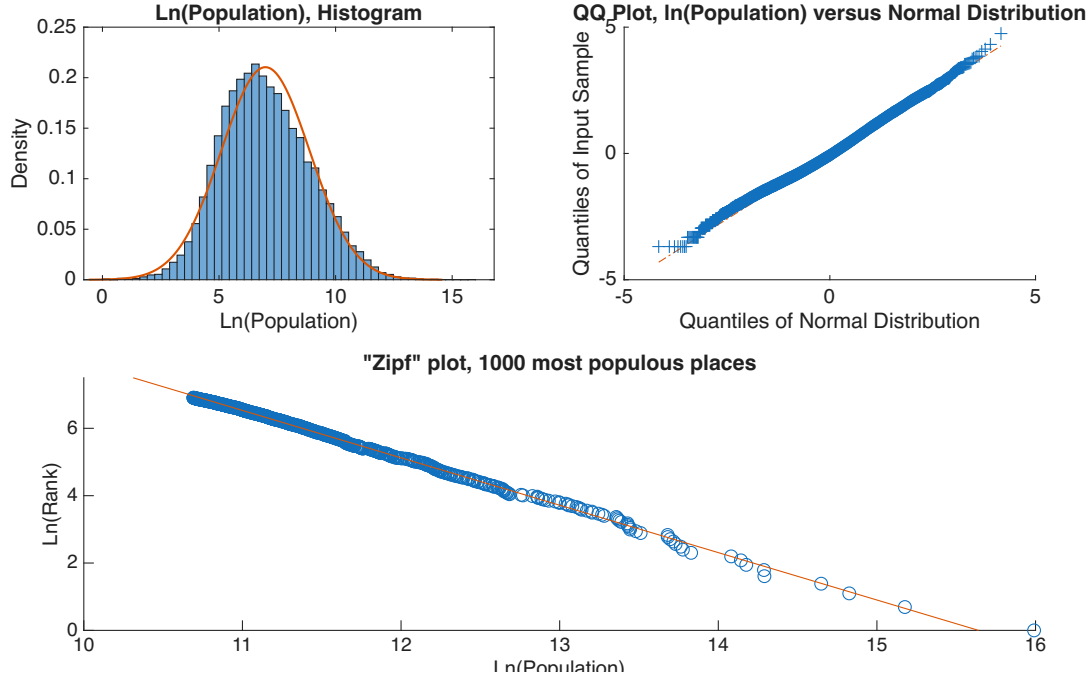
## 2 Seeing a Power Law in Populations

The appearance of a power law-like distribution for city populations is a well-documented feature of human geography. As articulated in Gabaix (1999b), the regularity of its appearance across countries, the definition of a “city,” and time mean that it can reasonably be held as a minimum criterion for a model of cities. This distribution is typically illustrated with a simple plot and accompanying regression. For some truncation of the population distribution to include only the most populous locations (“cities”), the plot of the log pop-

---

<sup>5</sup>Davis and Weinstein (2002) propose geography as a likely determinant of the population distribution, given the recovery of the cities to their prior place in the population distribution following devastating bombings.

**Figure I:** Lognormal Populations Appear to Follow A Power Law in the Tail



*Notes:* The populations of U.S. Incorporated and Census Designated Places ( $N = 31,430$ , U.S. Census Bureau 2020) appear to follow a lognormal distribution. The right tail of this distribution ( $N=1000$ ) appears to follow a power law.

ulation rank of a city and the log population of the city often appears strikingly linear and a regression given by:

$$\ln(\text{city rank}_i) = \theta_0 + \theta_1 \ln(\text{city pop}_i) + \epsilon_i \quad (1)$$

for many countries delivers a high  $R^2$  and frequently an estimate for  $\theta_1$  near -1. This slope is characteristic of a specific power law referred to as Zipf's Law, which can be stated as the largest city in a given country being  $n$  times the size of the  $n^{th}$ -largest city, and the frequent appearance of this "law" motivated a substantial literature seeking to explain its origin. Interpreting this regression as describing the true city size distribution would mean that city populations follow a Pareto distribution with shape parameter  $\alpha_P = 1$  and minimum city size  $x_m$ , reflecting the choice of truncation point.<sup>6</sup> A plot of this characteristic power

---

<sup>6</sup>The estimate of  $\theta_1 = -1$  means the power law is such that for size  $X$ , the probability that a city is larger than  $X$  is proportional to  $\frac{1}{X}$ . A Pareto distribution with shape parameter  $\alpha_P = 1$  and minimum city size  $x_m$  gives the necessary  $P(x > X) = \frac{x_m}{X}$ , which is the Pareto counter-cumulative distribution function for this  $\alpha_P$ . The link between the (log) rank-size plot and the Pareto distribution is established in more detail in Gabaix (2009).

law-like distribution can be seen in the bottom panel of Figure I, and in Appendix Figure A.II we provide a plot for U.S. MSAs that exhibits the same tendency.

Instead of being a true power law, the city size distribution may result from cities being a subset of a full population distribution which appears similar to a Pareto distribution for tail observations. Eeckhout (2004) demonstrates that the full population distribution for the U.S. appears lognormal. We construct an update to one of the key figures of Eeckhout (2004) in the upper panels of Figure I, which shows that this continues to hold for the U.S. in 2020. The top left panel shows a histogram of log population, which closely matches the overlaid normal distribution matching the mean and standard deviation of the empirical distribution, and the top right panel shows a close fit to the normal distribution in a quantile-quantile (QQ) plot. The right tail of this distribution, shown in the bottom panel, appears to closely follow a power law. These patterns are not unique to the level of geographic aggregation used in Figure I, to the U.S., or to countries. We show strikingly similar population distributions for a division of the U.S. into equal area geographies in Appendix B.2, and for Soviet Republics and their post-Soviet successor states in Appendix B.3.

The tail of a lognormal distribution often appears similar to a Pareto distribution, which can be understood by considering the lognormal PDF:

$$f(x) = \frac{1}{x\sigma\sqrt{2\pi}} \exp\left(-\frac{(\ln(x) - \mu)^2}{2\sigma^2}\right) \quad (2)$$

After some algebra (given in Supplemental Appendix A.1), this can be rewritten as:

$$f(x) = \Gamma_{LN} x^{-\alpha(x)-1} \quad (3)$$

where  $\Gamma_{LN} = \frac{1}{\sigma\sqrt{2\pi}} \exp\left(-\frac{\mu^2}{2\sigma^2}\right)$  and  $\alpha(x) = \frac{\ln(x) - 2\mu}{2\sigma^2}$ . Contrast this with the density function of a Pareto distribution:

$$j(x) = \Gamma_P x^{-\alpha_P-1} \quad (4)$$

where  $\Gamma_P = \alpha_P x_m^{\alpha_P}$  and the minimum city population is denoted  $x_m$ . The lognormal PDF in Equation 3 is similar to the Pareto density function in Equation 4, but with a scale-varying “shape parameter”-like term. As Malevergne et al. (2011) show, provided the  $\sigma$  parameter is not too small, the value  $\alpha(x)$  takes in the right tail will be stable over much of the tail distribution as  $\alpha(x)$  grows logarithmically in  $x$ .

The Pareto interpretation of the tail of the population distribution appears dominant in the literature despite its limitations and the strict assumptions it necessitates. First, the Pareto distribution is taken to apply to only a subset of large settlements and not the full

population distribution. This requires truncating a data series with no obvious truncation point. Early studies were limited to only the largest cities or settlements because of the comparative ease of accessing population counts for the largest places.<sup>7</sup> With more complete data on population distributions, the choice of a truncation point to support the Pareto interpretation becomes critical and there is no widely accepted method for determining such a cutoff. Many researchers rely on a visual test of the data to determine a cutoff (Gabaix 2009). Second, beyond the need to truncate the data to fit a Pareto distribution, models generating a Pareto population distribution must rely on strong assumptions regarding city growth dynamics. For example, Gabaix (1999b) obtains a Pareto distribution by assuming that cities cannot fall below a certain minimum size such that the otherwise random growth process is “reflected” at the lower bound. Third, the systematic deviations of the far right tail below the Pareto distribution observed in many countries (evident when considering U.S. MSAs, as in Appendix Figure A.II) are very large in magnitude, which is obscured by the log-log scale. We quantify the scale of these deviations in Supplemental Appendix B.<sup>8</sup>

The lognormal interpretation’s attractive properties stand in direct contrast to the shortcomings of the Pareto. The lognormal distribution appears to fit both the body of the population distribution as well as the right tail, obviating the need for arbitrary truncation. Further, the scale-varying “shape parameter”-like term of the lognormal (as shown in Equation 3) can explain commonly observed deviations in real-world city size distributions. The likelihood of very large cities is lower when the true distribution is lognormal than for a similar Pareto, because the scale-varying “shape parameter”-like term is increasing in  $x$ . This appears to match the global city distribution (Rossi-Hansberg and Wright 2007), as the largest cities in most countries tend to fall below the slope of the fitted regression line.<sup>9</sup> Other features of real-world population distributions, such as the sensitivity of the estimated slope to the choice of truncation point, are consistent with the lognormal

---

<sup>7</sup>This is true of early work, such as Auerbach (1913) and Zipf (1949). While Auerbach had data on many small settlements, a table in his paper includes just the 94 largest; see the recent translation in Auerbach and Ciccone (2023). Even more recent investigation of Zipf’s Law in Krugman (1996), for instance, included just the top 135 cities as the *Statistical Abstract of the United States* included only those cities (Eeckhout 2004).

<sup>8</sup>Estimating the Pareto coefficient on U.S. MSAs, the deviation below the implies a cumulative absence (in expectation) of nearly 76 million people from the 250 U.S. MSAs in Figure A.II, roughly a quarter of the U.S. population. Alternative estimates of the power law based on different truncation points imply as many as 500 million “missing” people in the largest U.S. MSAs, substantially more than the entire U.S. population.

<sup>9</sup>Proponents of the Pareto interpretation have attempted to accommodate this divergence by arguing that the forces acting on small cities are different from those acting on large cities, generating different power laws for different sizes of cities. A lognormal distribution naturally exhibits this deviation without the need to treat subsets of the distribution differently. We provide a further discussion of the scale variance of the lognormal distribution and its contrast with the Pareto distribution in Supplemental Appendix B.

distribution as well.<sup>10</sup>

The weight of evidence suggests that the appearance of a power law-like city population distribution is likely the result of focusing on the tail of a lognormal full population distribution. Such an interpretation requires fewer restrictive assumptions and appears to better fit the observed data, both in the body of the population distribution (which is necessarily ignored by the Pareto interpretation) and in the tail (which behaves more lognormal than Pareto).

### 3 Lognormal Populations in Spatial Models

We now describe the canonical quantitative spatial model within which we demonstrate our key result. We use a discretized version of the model in Allen and Arkolakis (2014), which nests the canonical class of spatial models, and show that a realistic modeling of geography and trade will lead to lognormal population distributions in equilibrium.<sup>11</sup>

#### 3.1 A Quantitative Spatial Equilibrium Model

The world consists of locations indexed by  $i \in \mathcal{N}$ , where  $\mathcal{N} = \{i \mid i \in \mathbb{Z}^2, (-N, -N) \leq i \leq (N, N)\}$  where  $N \in \mathbb{N}$  determines the extent of the plane. Trade between different locations is costly. We assume that locations have symmetric iceberg trade costs drawn from some distribution with finite support, such that  $\tau_{i,i} = 1$ ,  $\tau_{s,t} > 1$  for  $s \neq t$ ,  $\tau_{s,t} = \tau_{t,s}$ , and trade costs between any pair of locations  $s, t \in \mathcal{N}$  are bounded above by a positive number.

The “distance” between locations is defined using the Euclidean norm such that  $d_{i,j} = \|i - j\|$ . Distance is distinct from trade costs. Locations that are near each other will tend to be similar (in a sense to be made more precise in the following section) because of spatial correlation in geography, while trade costs can vary independently of distance to reflect varied geographies, trade routes linking certain distant locations (navigable rivers, railways, roads, etc.), or other idiosyncratic barriers to trade between locations.

Each location has an exogenous productivity fundamental  $A_i$  and an exogenous amenity

---

<sup>10</sup>This property is discussed at length in Eeckhout (2004) and demonstrated in Supplemental Appendix Figure A.III where we expand or reduce the number of cities relative to Figure A.II. The sensitivity to the truncation point and the lack of a reliable rule for truncating the distribution suggest that the frequently estimated -1 exponent is unlikely to be a meaningful feature of the data. For some truncation of tail observations drawn from many lognormal distributions, the log-rank log-population plot will appear to take a slope of -1 as the exponent in Equation 3 diverges smoothly.

<sup>11</sup>The Allen and Arkolakis (2014) model is based on the two-location model presented in Helpman (1998), generalized to an arbitrary number of locations.

fundamental  $U_i$ , both of which are strictly positive, real-valued random variables drawn from some probability distribution. We discuss the fundamentals further later in this section, where we argue that these should reflect variation in the attributes of a place and the spatial correlation patterns of attributes across space. A location's effective productivity and amenity value may also be affected by negative or positive externalities due to the local population  $L_i$ . We define the "composite fundamentals" as:

$$\tilde{A}_i = A_i L_i^\alpha \quad (5)$$

$$\tilde{U}_i = U_i L_i^\beta \quad (6)$$

where the typical case will consist of  $\alpha > 0$  and  $\beta < 0$ , reflecting positive productivity spillovers from agglomeration and the negative impact of overcrowding on amenities. Geography within this model is represented by the set of functions defining the locational fundamentals,  $\tilde{A}_i$  and  $\tilde{U}_i$ , along with the trade costs function  $\tau$  defining the spatial relationship between locations in the model.

We make the Armington assumption that each location produces a differentiated good. There is a population of homogeneous workers  $\bar{L} \in \mathbb{R}_{++}$  who can freely move to any location. Workers have common constant elasticity of substitution preferences over goods in their welfare function given by:

$$W_i = \left( \sum_{n \in \mathcal{N}} q_{n,i}^{\frac{\sigma-1}{\sigma}} \right)^{\frac{\sigma}{\sigma-1}} \tilde{U}_i \quad (7)$$

where  $\tilde{U}_i$  is the composite amenity fundamental of location  $i$  and  $q_{n,i}$  denotes the total consumption in  $i$  of the good produced in  $n$  and  $\sigma > 1$  governs the elasticity of substitution.

Production is perfectly competitive.<sup>12</sup> A worker in location  $i$  can produce  $\tilde{A}_i$  units of the local differentiated good, where  $\tilde{A}_i$  is the composite productivity fundamental of location  $i$ . The number of workers and wages in a location are given by the functions  $L : N \rightarrow \mathbb{R}_{++}$  and  $w : N \rightarrow \mathbb{R}_{++}$ .<sup>13</sup>

Based on the CES assumption, we can write the amount of each good produced in any location  $i$  consumed in location  $n$  as:

$$q_{i,n} = Q_n \left( \frac{p_{i,n}}{P_n} \right)^{-\sigma} \quad (8)$$

---

<sup>12</sup>As demonstrated in the appendix to Allen and Arkolakis (2014), the model nests cases of monopolistic competition.

<sup>13</sup>All locations will be populated and offer positive wages in equilibrium given the range of parameters we consider.

where  $Q_n$  is aggregate consumption in  $n$ ,  $Q_n = \frac{w_n L_n}{P_n}$ , and  $P_n$  is the price index in location  $n$ , given by:

$$P_n = \left( \sum_{i \in \mathcal{N}} p_{i,n}^{1-\sigma} \right)^{\frac{1}{1-\sigma}} \quad (9)$$

Given the assumption of perfect competition the price of the good produced in  $i$  consumed in  $n$ , can be expressed as:

$$p_{i,n} = \frac{\tau_{i,n} w_i}{\tilde{A}_i} \quad (10)$$

Combining the quantity (Equation 8) and price (Equation 10) expressions, we can write the value of the good produced in  $i$  consumed by  $n$  as:

$$X_{i,n} = \left( \frac{\tau_{i,n} w_i}{\tilde{A}_i P_n} \right)^{1-\sigma} w_n L_n \quad (11)$$

By the CES assumption we can express the welfare of a worker in each location as:

$$W_i = \frac{w_i}{P_i} \tilde{U}_i \quad (12)$$

The total income in a location must be equal to the value of production:

$$w_i L_i = \sum_{n \in \mathcal{N}} X_{i,n} \quad (13)$$

The labor market clears:

$$\sum_{n \in \mathcal{N}} L_n = \bar{L} \quad (14)$$

We can then combine the welfare expression (Equation 12), value of consumption expression (Equation 11), and income expression (Equation 13) to get:

$$L_i w_i^\sigma = \sum_{n \in \mathcal{N}} W_n^{1-\sigma} \tau_{i,n}^{1-\sigma} \tilde{A}_i^{\sigma-1} \tilde{U}_n^{\sigma-1} L_n w_n^\sigma \quad (15)$$

The welfare expression (Equation 12) combined with the price index and prices (Equations 9 and 10) yields:

$$w_i^{1-\sigma} = \sum_{n \in \mathcal{N}} W_i^{1-\sigma} \tau_{n,i}^{1-\sigma} \tilde{A}_n^{\sigma-1} \tilde{U}_i^{\sigma-1} w_n^{1-\sigma} \quad (16)$$

Given the form of the externalities in Equations 5 and 6, free movement between locations which ensures worker welfare is equal in all locations ( $W_i = \bar{W}$  for all  $i$ ), and symmetric

trade costs we can combine Equations 15 and 16 into a single equation given by:

$$L_i^{\tilde{\sigma}\gamma_1} = \bar{W}^{1-\sigma} A_i^{\tilde{\sigma}(\sigma-1)} U_i^{\tilde{\sigma}\sigma} \sum_{n \in \mathcal{N}} \tau_{n,i}^{1-\sigma} U_n^{\tilde{\sigma}(\sigma-1)} A_n^{\tilde{\sigma}\sigma} (L_n^{\tilde{\sigma}\gamma_1})^{\frac{\gamma_2}{\gamma_1}} \quad (17)$$

where:

$$\tilde{\sigma} = \frac{\sigma - 1}{2\sigma - 1}, \quad \gamma_1 = 1 - \alpha(\sigma - 1) - \beta\sigma, \quad \gamma_2 = 1 + \alpha\sigma + (\sigma - 1)\beta$$

The existence and uniqueness of the equilibrium, and a mechanism for finding it, are established in Allen and Arkolakis (2014) when  $\frac{\gamma_2}{\gamma_1} \in (-1, 1]$  (the discrete case is considered in their online appendix). We focus on this part of the parameter space, which occurs when  $\alpha + \beta \leq 0$  and is the empirically relevant case.

We now demonstrate that the equilibrium population within this model will be lognormally distributed given a realistic modeling of the fundamentals based on random variation across and within locations in their attributes, as well as variation in trade costs. We begin by rewriting Equation 17 in terms of the population in each location  $i$  in simplifying notation as:

$$L_i = F_i \times M_i^{\frac{1}{\tilde{\sigma}\gamma_1}} \quad (18)$$

where  $F_i = (\bar{W}^{1-\sigma} A_i^{\tilde{\sigma}(\sigma-1)} U_i^{\tilde{\sigma}\sigma})^{\frac{1}{\tilde{\sigma}\gamma_1}}$ , which we refer to as the “own-fundamental” term as it consists only of location  $i$ ’s fundamentals and the common positive constant  $\bar{W}$ , and  $M_i = \sum_{n \in \mathcal{N}} m_{n,i}$  with  $m_{n,i} = \tau_{n,i}^{1-\sigma} U_n^{\tilde{\sigma}(\sigma-1)} A_n^{\tilde{\sigma}\sigma} L_n^{\tilde{\sigma}\gamma_2}$ , which we refer to as the “market access” term of location  $i$  as it is a trade cost-weighted sum over all locations  $n \in \mathcal{N}$ . Each term  $m_{n,i}$  of this summation thus represents the contribution of location  $n$  to the market access of location  $i$ .

We now demonstrate that, given a realistic modeling of variation across space and within a place, both the own-fundamental and market access terms for all locations will be lognormally distributed. This will allow us to show that the equilibrium population also follows a lognormal distribution.

### 3.2 Variation within Place and the Distribution of Fundamentals

We model fundamentals as resulting from random shocks via the attributes of a location, building on the approach of Lee and Li (2013) who similarly model a location’s quality as resulting from many random “factors.” We reframe their approach as modeling fundamentals as arising from variation in local attributes due to variation in geography. Using random variation in the attributes of a location to model locational fundamentals is the cross-sectional analog of random growth models based on Gibrat’s law over time, like

those of Gabaix (1999a) and Eeckhout (2004), where rather than productivity shocks occurring over time each attribute within a location contributes a productivity or amenity shock to each locational fundamental.

There is clear evidence for observable geographic attributes, alone and in combination, playing a role in shaping human settlement patterns (Henderson et al. 2018). The substantial differences between areas of high population in terms of many geographic attributes suggest that no one particular observable attribute alone is a sufficient proxy for what makes a location good for human habitation, and that many attributes should contribute to the quality of a place.

Each location  $i$  has many geographic attributes  $a_{ig}$ , which are indexed by  $g \in \mathcal{G}$ , where  $\mathcal{G} = \{g \mid g \in \mathbb{N}, 1 \leq g \leq G\}$ . Attributes for a productive location could be fertile soil, regular and mild weather patterns, and favorable topography, among many others. We assume all attributes are strictly positive in value any  $g$ .<sup>14</sup> We also assume each individual attribute is drawn from a common distribution in all locations, while different attributes may differ in their respective distribution.

We focus our discussion on productivity fundamentals, as we define the amenity fundamentals in the same way. The locational productivity fundamental for a location  $i$ , denoted  $A_i$ , should be a function of its many attributes such that  $A_i = F_A(a_{i1}, a_{i2}, \dots, a_{iG})$ . This function should be increasing in each  $a_{ig}$ , to reflect that better attributes increase productivity, such that  $\frac{\partial F_A}{\partial a_{ig}} > 0$  for all  $g \in \mathcal{G}$ . Further, the aggregating function should exhibit complementarities between each of the attributes. That is, the benefit of having reliable rainfall for production is increased when there is better arable land in a location, for instance. This means the aggregating function also needs a positive cross-partial for all arbitrary combinations of attributes, such that  $\frac{\partial^2 F_A(\cdot)}{\partial a_{ij} \partial a_{ig}} > 0$ , for  $j, g \in \mathcal{G}, j \neq g$ .

Consistent with these assumptions, we can view the contribution of attributes to the fundamental as representing multiplicative shocks. We assume a Cobb-Douglas form for the aggregating function  $F_A$ , consistent with the requirements outlined above. The varying importance of different attributes can be reflected by the exponents  $\xi_g$  associated with each  $g$ :<sup>15</sup>

$$A_i = \prod_{g \in \mathcal{G}} a_{ig}^{\xi_g} \quad (19)$$

---

<sup>14</sup>These should not be thought of as being measured in the familiar units for each attribute. Rainfall in inches has a nonlinear relationship with agricultural output, for instance. We instead want a measure reflecting how positive the “shock” from a given attribute is.

<sup>15</sup>We could also include an index for the time  $t$ , to allow for attributes  $a_{igt}$  to vary over time and to vary in their importance over time  $\xi_{gt}$ , which could capture structural transformation of the economy or changing production technologies at time  $t$ . In this case,  $A_{it} = \prod_{g \in \mathcal{G}} a_{igt}^{\xi_{gt}}$  where the fundamentals can vary with  $t$ .

Taking the natural log yields the following expression:

$$\ln(A_i) = \sum_{g \in \mathcal{G}} \xi_g \ln a_{ig} \quad (20)$$

where we express the logged fundamental in location  $i$  as a sum of random variables  $\xi_g \ln a_{ig}$ .

It is possible that some attributes  $a_{ig}$  are not independent within locations. For example, high July temperatures and the number of growing days may be correlated within places such that knowing the realization of one is informative about the likely values of the other. However, over the large number of attributes of a place there do appear to exist pairs of attributes which appear nearly independent within locations (e.g., topography and rainfall), as we demonstrate in Supplemental Appendix C.4 using data on geographic attributes from Henderson et al. (2018).

Many modern central limit theorems allow for precisely this type of asymptotic independence. The formal assumption we must impose in order to apply a central limit theorem is that the sequences must be  $\alpha$ -mixing for each  $i \in \mathcal{N}$ . This concept, also referred to as “strong mixing” or “weak dependence,” was introduced to the spatial literature in Lee and Li (2013). A formal definition of  $\alpha$ -mixing for sequences is given below. The concept requires that all events defined on arbitrary subsets of an  $\alpha$ -mixing sequence approach independence as the “distance” between the subsets increases, where distance is reflected in the index of the sets. This concept is often used in the analysis of time series, where the index reflects the timing of the observation and imposes a natural concept of the distance between elements of the sequence.

**Definition 1,  $\alpha$ -mixing (sequences):** Suppose  $X := (X_k, k \in \mathbb{Z})$  is a (not necessarily stationary) sequence of random variables. For  $-\infty \leq J \leq L \leq \infty$ , define the  $\sigma$ -field

$$\mathcal{F}_J^L := \sigma(X_k, J \leq k \leq L | k \in \mathbb{Z}).$$

The notation  $\sigma(\dots)$  means the  $\sigma$ -field  $\subset \mathcal{F}$  generated by  $(\dots)$ . Define:

$$\alpha(\mathcal{F}_{-\infty}^j, \mathcal{F}_{j+n}^\infty) = \sup_{A \in \mathcal{F}_{-\infty}^j, B \in \mathcal{F}_{j+n}^\infty} |\mathbb{P}(A \cap B) - \mathbb{P}(A)\mathbb{P}(B)|.$$

For each  $n \geq 1$ , define:

$$\alpha(n) := \sup_{j \in \mathbb{Z}} \alpha(\mathcal{F}_{-\infty}^j, \mathcal{F}_{j+n}^\infty),$$

The random sequence  $X$  is said to be “strongly mixing” (or “ $\alpha$ -mixing”) if  $\alpha(n) \rightarrow 0$  as  $n \rightarrow \infty$ .

We assume that attributes satisfy these properties and are  $\alpha$ -mixing within locations. Given this assumption, we write Lemma 1. Lemma 1 is a central limit theorem for  $\alpha$ -mixing sequences due to Herrndorf (1984). It allows us to demonstrate convergence of a sum over a sequence of non-i.i.d. random variables to a normal distribution, provided asymptotic independence (given by  $\alpha$ -mixing) and other moment conditions for the sequence.

**Lemma 1 (Herrndorf 1984):** Let  $\{x_i\}$  be an  $\alpha$ -mixing sequence of random variables satisfying the following conditions:

- i.  $\mathbb{E}[x_i] = 0, \forall i$
- ii.  $\lim_{n \rightarrow \infty} \frac{\mathbb{E}[(\sum_{i=1}^n x_i)^2]}{n} = \bar{\sigma}^2, 0 < \bar{\sigma}^2 < \infty$
- iii.  $\sup_{i \in \mathcal{N}} \mathbb{E}[x_i^b] < \infty$ , for some  $b > 2$
- iv.  $\sum_{s=1}^{\infty} (\alpha_s)^{1-\frac{2}{b}} < \infty$

Let  $X_n = \sum_{i=1}^n x_i$ . Then as  $n \rightarrow \infty$ ,  $\frac{1}{\sqrt{n}\bar{\sigma}} X_n$  converges in distribution to the standard normal distribution.

The proof of Lemma 1 is given in Herrndorf (1984), and a discussion of the conditions is given in Lee and Li (2013).

We define the ordering of the sequence of attributes  $\{a_{i1}, a_{i2}, \dots, a_{iG}\}$  such that similar attributes are close together (July temperatures and growing days have indices near each other) to create  $\alpha$ -mixing sequences of these attributes. Together with further restrictions, given in Lemma 1, on the moments of the random variables  $\xi_g \ln a_{ig}$  and the rate of  $\alpha$ -mixing, which determines how rapidly the elements of the sequence approach independence, we apply the central limit theorem in Lemma 1 to characterize the distribution of each  $\ln A_i$ .

**Proposition 1:** Define  $\widehat{\xi_g \ln a_{ig}} = \widehat{\xi_g} \ln a_{ig} - \mathbb{E}[\xi_g \ln a_{ig}]$  for all  $g \in \mathcal{G}$  and  $i \in \mathcal{N}$ , and define  $\widehat{\ln A_i} = \sum_{g \in \mathcal{G}} \widehat{\xi_g \ln a_{ig}}$  and  $\sigma(\widehat{\ln A_i})^2 = \text{Var}[\widehat{\ln A_i}]$  for all  $i \in \mathcal{N}$ . If the sequences  $\{\widehat{\xi_g \ln a_{ig}}\}$  are  $\alpha$ -mixing and fulfill the conditions of Lemma 1 for all  $i \in \mathcal{N}$ , then as  $G \rightarrow \infty$ ,  $\frac{1}{\sqrt{G}\sigma(\widehat{\ln A_i})} \widehat{\ln A_i}$  converges in distribution to the standard normal distribution for all  $i \in \mathcal{N}$ .

Proposition 1 follows from Lemma 1. By Proposition 1, as the number of attributes grows large, the log productivity fundamental  $\ln A_i$  will converge in distribution to a normal distribution and so  $A_i$  will converge in distribution to a lognormal distribution. We assume that, for a large number of attributes,  $A_i$  will be lognormally distributed based on this asymptotic argument.

The amenity fundamental is defined similarly, but we allow for different weights as the attributes most relevant for determining quality of life may differ from those influencing productivity. The log of the amenity fundamental, which has weights given by  $\iota_g > 0$ , is:

$$\ln(U_i) = \sum_{g \in \mathcal{G}} \iota_g \ln a_{ig} \quad (21)$$

and, given the same conditions as on the productivity fundamental established in Proposition 1 and Lemma 1, will also converge in distribution to a lognormal as the number of attributes grows large.

Given lognormally distributed productivity and amenity fundamentals  $A_i$  and  $U_i$ , we can show that the “own-fundamental” term  $F_i = (\bar{W}^{1-\sigma} A_i^{\tilde{\sigma}(\sigma-1)} U_i^{\tilde{\sigma}\sigma})^{\frac{1}{\tilde{\sigma}\gamma_1}}$  for each location  $i$  will be lognormally distributed.

**Proposition 2:** *If  $A_i$  and  $U_i$  have a bivariate normal distribution in logs,  $F_i$  will be lognormally distributed.*

Proposition 2 follows immediately from the properties of lognormals, as either raising a lognormal distribution to a power or multiplying by a positive constant begets another lognormally distributed random variable and multiplying two lognormal random variables which have a bivariate normal distribution in logs also results in another lognormally distributed random variable.

We provide empirical support for the appearance of a lognormal distribution for fundamentals. We use the Henderson et al. (2018) data on attributes and, following our modeling assumptions, calculate a “naive” fundamental by applying our aggregating function.<sup>16</sup> The plot is reported in Supplemental Appendix C.6, and show that aggregating the eleven attributes results in a distribution of fundamentals that appears lognormal. While only suggestive, the construction of a “naive” fundamental from attributes result in strikingly lognormal distributions, despite the high degree of correlations in attributes that we document.

### 3.3 Variation over Space and the Distribution of Market Access

We now demonstrate that the market access term, which is a summation over positive random variables, will converge in distribution to a lognormal as the number of locations

---

<sup>16</sup>We say the fundamental is “naive” in the sense that we do not know the appropriate weights or scaling of the attributes. The construction of the fundamental is discussed in Supplemental Appendix C.5. A similar exercise was earlier done by Behrens and Robert-Nicoud (2015) for U.S. MSAs.

in the model grows large. This result follows from the application of Lemma 1's  $\alpha$ -mixing central limit theorem, as there may be correlation over space between elements of the market access summation, and a useful lemma due to Marlow (1967) for sums of positive random variables.

The market access term for each location  $i$  is a summation defined across locations  $n \in \mathcal{N}$  given by  $M_i = \sum_{n \in \mathcal{N}} m_{n,i}$ , where each  $m_{n,i} = \tau_{n,i}^{1-\sigma} U_n^{\tilde{\sigma}(\sigma-1)} A_n^{\tilde{\sigma}\sigma} L_n^{\tilde{\sigma}\gamma_2}$  is a function of the trade costs between  $n$  and  $i$  and each location  $n$ 's fundamentals and population. As these  $M_i$  are summations of random variables, we will again use a central limit theorem to characterize the distribution of this sum as we did for the aggregates of attributes within locations.<sup>17</sup> We will similarly need to contend with potential correlation in these random variables, in this case across space rather than within a place. The similarity of nearby locations is a reliable feature of the world, and has been framed as the "first law of geography." As stated by Tobler (1970), this law holds that "everything is related to everything else, but near things are more related than distant things."

Nearby locations often have broadly similar geographic attributes, like the climatic similarities of New York City and northern New Jersey, but this spatial correlation declines with distance such that New York City is quite dissimilar from both Monterrey, Mexico, and Nuuk, Greenland.<sup>18</sup> As the locational fundamentals are aggregates of spatially correlated geographic attributes, which we quantify in Appendix C.4 based on the geographic attributes data in Henderson et al. (2018), these fundamentals are very likely to themselves be correlated across space. Given the similarity in locational fundamentals for nearby locations, the populations of nearby locations may also be correlated. Trade costs may also be similar from a given  $i$  to any pair of  $n, m \in \mathcal{N}$ , where  $n$  and  $m$  are located near each other.

Importantly, though, this correlation decays across space. Again, the first law of geography states that "near things are more related than distant things," and as distance increases the correlation in attributes we document in Appendix C.4 declines to zero. This decline with increasing distance is consistent with the assumption of  $\alpha$ -mixing across space for the elements of our market access summation, which we use to apply a central limit theorem to this summation. We have a clear definition of distance between locations in our setting given by  $d_{n,i}$ . We can re-index the elements of the market access summation sequence  $\{m_{n,i}\}$  in terms of distance by defining for each  $i$  an alternative sequence ordered by distance from  $i$ ,  $\{m_{j,i}^d\}$ , where  $m_{1,i}^d = m_{i,i}$  (at a distance of 0) is followed by

---

<sup>17</sup>In Appendix A.4 we motivate the treatment of  $L_n$  as random variables, because each  $L_n$  is an element of a random sequence corresponding to the eigenvector of a random matrix.

<sup>18</sup>Nuuk and Monterrey are roughly equidistant from New York City, both at a distance of 1,850 miles.

locations  $m_{2,i}^d$  capturing locations at the next nearest distance, and so on, with ties broken arbitrarily. Note that as the sequences  $\{m_{j,i}^d\}$  are simply a re-indexing of the sequences  $\{m_{n,i}\}$ ,  $M_i = \sum_{n \in \mathcal{N}} m_{n,i} = \sum_{j \in \mathcal{N}} m_{j,i}^d$  for all  $i \in \mathcal{N}$ . We assume that the sequences  $\{m_{j,i}^d\}$  are  $\alpha$ -mixing for all  $i \in \mathcal{N}$  to reflect asymptotic independence with respect to distance.

An additional property of the summations  $M_i$  allows us to move from a central limit theorem in levels to one in logs, which will allow us to characterize the distribution of  $M_i$  as lognormal. Each  $m_{n,i}$  must be strictly positive, as  $A_n, U_n, \tau_{n,i}$ , and  $L_n$  are all strictly positive and so  $m_{n,i} = \tau_{n,i}^{1-\sigma} U_n^{\tilde{\sigma}(\sigma-1)} A_n^{\tilde{\sigma}\sigma} L_n^{\tilde{\sigma}\gamma_2} > 0$ . This allows us to apply a useful lemma from Marlow (1967), which provides conditions under which a lognormal distribution may appear from a summation of positive random variables:

**Lemma 2 (Marlow 1967):** *Let  $\{X_n\}$  be a sequence of positive random variables. Suppose there exist sequences of positive real numbers  $\{a_n\}$  and  $\{b_n\}$ , and a distribution  $F$  such that*

- i. *At each point of continuity of  $F$ ,  $\lim_{n \rightarrow \infty} P \left\{ \frac{X_n - a_n}{b_n} \leq x \right\} = F(x)$*
- ii.  $\lim_{n \rightarrow \infty} \left( \frac{b_n}{a_n} \right) = 0$

*Then at each point of continuity of  $F$ ,  $\lim_{n \rightarrow \infty} P \left\{ \left( \frac{a_n}{b_n} \right) \ln \left( \frac{X_n}{a_n} \right) \leq x \right\} = F(x)$*

The proof of Lemma 2 is given in Marlow (1967). Condition (i) can reflect convergence under a central limit theorem (such as Lemma 1), where  $F(x)$  is the standard normal distribution and the sequences  $a_n$  and  $b_n$  are the mean and standard deviation of some  $X_n$  resulting from a sum of random variables. Condition (ii) then necessitates that the coefficient of variation (the ratio of the standard deviation to the mean) of  $X_n$  is zero in the limit as  $n$  grows large. Many sums of positive random variables fulfill this requirement, and we provide several examples in Supplemental Appendix A.2.

Lemma 2 allows us to apply a central limit theorem to the sum  $M_i$  for all  $i \in \mathcal{N}$ , provided the sequences  $\{m_{n,i}^d\}$  fulfill the requirements of the lemma. For a sum that satisfies the conditions for a central limit theorem and condition (ii), Lemma 2 states that the given normalization of the sum will converge in distribution to a lognormal random variable.<sup>19</sup> Lemma 2 is crucial for understanding the population distribution within many spatial equilibrium models, as these models often incorporate a notion of “market access” via a trade cost-weighted sum over all locations. All of the elements of these sums must be strictly positive, and provided these fulfill the conditions necessary for applying a central

---

<sup>19</sup>We discuss Lemma 2 further in Supplemental Appendix A.2. Beyond the context in which we apply the Marlow (1967) lemma, it appears to have broad usefulness within economics. For example, a CES aggregator over positive random variables fulfilling the conditions of the lemma should approach lognormality as the lognormal distribution is preserved over exponentiation.

limit theorem and Lemma 2 the distribution of these “market access” terms will approach a lognormal distribution as the number of locations grows large. We state this result in Proposition 3.

**Proposition 3:** For each  $i \in \mathcal{N}$ , define the sequences  $\{m_{1,i}^d, m_{2,i}^d, \dots, m_{N,i}^d\}$  and the demeaned sequences  $\{\hat{m}_{n,i}^d\}$  such that  $\mathbb{E}[\hat{m}_{n,i}^d] = 0$  for all  $n \in \mathcal{N}$ . Define  $M_i^{(N)} = \sum_{n=1}^N m_{n,i}^d$ ,  $\mu_i^{(N)} = \sum_{n=1}^N \mathbb{E}[m_{n,i}^d]$ , and  $\sigma(M_i^{(N)})^2 = \text{Var}[M_i^{(N)}]$ . If, for all  $i$ ,

- i. The sequences  $\{\hat{m}_{1,i}^d, \hat{m}_{2,i}^d, \dots, \hat{m}_{N,i}^d\}$  are  $\alpha$ -mixing and fulfill the conditions in Lemma 1
- ii. The coefficients of variation associated with the sequences  $\{M_i^{(1)}, M_i^{(2)}, \dots, M_i^{(N)}\}$  fulfill condition (ii) of Lemma 2 as  $N \rightarrow \infty$

then  $\frac{\mu_i^{(N)}}{\sqrt{N}\sigma(M_i^{(N)})} \ln \left( \frac{M_i^{(N)}}{\mu_i^{(N)}} \right)$  converges in distribution to a normal distribution for all  $i$  as  $N \rightarrow \infty$ .

The proof follows directly from Lemma 1 and Lemma 2. Lemma 1 allows us to apply an  $\alpha$ -mixing central limit theorem to the sum  $M_i$ , and Lemma 2 allows us to move to a central limit theorem in logs as all elements of this sum are positive. If the necessary assumptions on  $m_{n,i}$  hold, the market access summation  $M_i$  converges in distribution to a lognormal as  $N$  grows large. As a lognormal raised to a power results in another lognormal distribution each  $(M_i)^{\frac{1}{\bar{\sigma}\gamma_1}}$  will converge in distribution to a lognormal distribution as  $N$  grows large.

It is important to note that this property of market access is not specific to the Allen and Arkolakis (2014) model. Any setting where market access is modeled as consisting of a summation over many locations should have this property, provided the conditions of the proposition and relevant lemmas hold, as market access will necessarily be made up of positive contributions from the incomes and populations of many locations.

Given the near certainty of substantial correlation in attributes and thus fundamentals across space, we would like to emphasize that variation in trade costs is likely a key criterion for the market access terms to fulfill the requirements of Proposition 3. Trade costs can vary substantially over short distances, either due to variation in access to natural features like rivers or oceans, being uphill or downhill, or due to the presence of transportation infrastructure. For two otherwise similar nearby locations, one may be along a trade route while the other is more costly to access. Consider a port city, in contrast to areas slightly further inland, or a railroad hub in contrast to other towns bypassed by the rail network. While many geographic attributes of the two may be similar, as land transportation is much more expensive than transportation by sea or rail the trade costs facing the port city will be systematically lower. This variation may be important for the Proposition’s assumptions to hold in the real world and ensure that market access follows a log normal distribution as the Proposition implies.

### 3.4 The Distribution of the Population

We have now shown that  $F_i$  and  $(M_i)^{\frac{1}{\bar{\sigma}\gamma_1}}$  are lognormally distributed when realistically modeled to reflect variation in geography and trade costs over space. Using this, we can then show that the population will be lognormally distributed as the population in each location  $i$  is given by  $L_i = F_i M_i^{\frac{1}{\bar{\sigma}\gamma_1}}$ . This result is given in Theorem 1.

**Theorem 1:** *If  $F_i$  and  $M_i^{\frac{1}{\bar{\sigma}\gamma_1}}$  have a bivariate normal distribution in logs for all  $i \in \mathcal{N}$ , then  $L_i$  follows a lognormal distribution for all  $i \in \mathcal{N}$ .*

The proof follows directly from the lognormality of  $F_i$  and  $M_i^{\frac{1}{\bar{\sigma}\gamma_1}}$ , and the property that products of lognormal distributions which have a bivariate normal distribution in logs also follow a lognormal distribution. Additional technical details regarding the ergodicity of the population distribution and spatial correlations are provided in Appendix A.3.

## 4 Results

We now verify our modeling assumptions by recovering fundamentals, inverting the model on U.S. data. The recovered fundamentals are lognormally distributed, supporting the modeling assumptions we made for these fundamentals and resulting in lognormal own-fundamental terms. The empirical market access terms we construct based on the theory and these recovered fundamentals are also lognormally distributed, as predicted by the theory.

We then test further features of the model in simulation. We show that for empirically relevant parameter values we achieve a good fit to a lognormal distribution in a finite setting, supporting the relevance of our asymptotic results. We provide simulated comparative statics based on varying parameter values across simulations to document how changes in congestion, spillovers, and trade costs influence the observed power law. We identify changes to the power law in the directions implied by the empirical literature. Finally, we note an additional theoretical result relating to the prior Zipf's law literature. Given the properties of the model, we show that Gibrat's law holds within the model when the aggregate population increases, showing that size-invariant growth is a feature of a lognormal equilibrium population distribution based on variation in geography and trade, in contrast to earlier literature that took random growth to be the basis for lognormal populations.

## 4.1 Model Inversion: Recovering lognormal fundamentals and market access

We now test the validity of our modeling assumptions and their predictions using data for U.S. counties. Using estimates for trade costs and data on local populations and wages, we invert the model to recover fundamentals and market access. We find that, as predicted, both fundamentals and market access follow lognormal distributions.

The geographic level at which we can perform the model inversion is limited by the availability of reliable data on populations and wages, along with the need to include the full U.S. population distribution. Note that the definition of a “location” is not specified by the model, beyond being a place within which local agglomeration and congestion spillovers occur.<sup>20</sup> The availability of trade data between U.S. regions is also limited to larger Commodity Flow Survey (CFS) regions, which are constructed from counties. We use the 2020 Decennial Census data for county-level populations and 2020 American Community Survey data on incomes to construct county-level wages and populations for the model inversion. We also use these data sources to construct measures of the similarity of counties and CFS regions for the trade costs estimation. We also draw on the 2020 County Business Patterns data to construct measures of the similarity of counties and CFS regions in terms of the sectoral composition of their economies. We repeat our inversion on alternative geographies in Appendix D and find similar results to our county-level inversion.

We follow the two-step trade cost estimation procedure as in Allen and Arkolakis (2014). We first recover trade costs parameters up to scale using the observed trade shares shipped by road, rail, and water in the 2017 Commodity Flow Survey to estimate a discrete choice model of trade. We construct travel maps from the Census TIGER/Line collection and the US Department of Transportation for these shipping modes, and estimate the distances between CFS regions from population-weighted county-county distances based on Head and Mayer (2009). We set the fixed cost of road shipping to 0 such that we recover the relative scaling of these trade costs. We then estimate a PPML regression of trade flows on the geographic trade costs from the first stage, along with non-geographic factors that may affect trade flows, to recover the remaining parameters of this discrete choice problem and appropriately scale trade costs. Further details about the data and our trade costs estimation procedure are given in Appendix D.

---

<sup>20</sup>That the model is ambiguous on the level of aggregation of population means it is consistent with the observation of the characteristic population distribution at varying levels of aggregation, as in Holmes and Lee (2010), Rozenfeld et al. (2011), and Mori et al. (2020). Spillovers are unlikely to be purely local at any level of aggregation, and so differing levels of aggregation may require different parameters governing “local” spillovers that are a useful abstraction from more complex patterns of spillovers.

Given these estimated trade costs between all counties, we are then able to invert the model and recover  $A_i$  and  $U_i$  for all U.S. counties. Our inversion procedure differs from that in Allen and Arkolakis (2014) in that we interpret  $L_i$  as the population of the counties rather than county population density. Our interpretation is consistent with equation 13, which states that total income in a location must equal its production. Interpreting  $L_i$  as population, rather than population density, also more closely matches the interpretation of the  $M_i$  term as reflecting market access.

Following the inversion, we recover the exogenous locational fundamentals by setting  $\alpha = 0.03$ , in line with the estimates in Combes et al. (2019), Rosenthal and Strange (2004), and Combes and Gobillon (2015). Using an isomorphism in the model based on the share of household spending on housing  $sh$  that gives  $\beta = \frac{1}{1-sh}$ , we fix  $\beta = -\frac{1}{3}$  given a value of  $sh = 25\%$ , consistent with estimates in Combes et al. (2008) and Davis and Ortalo-Magné (2011). We set  $\sigma = 5$ , as in Redding and Rossi-Hansberg (2017) based on estimates from Simonovska and Waugh (2014).

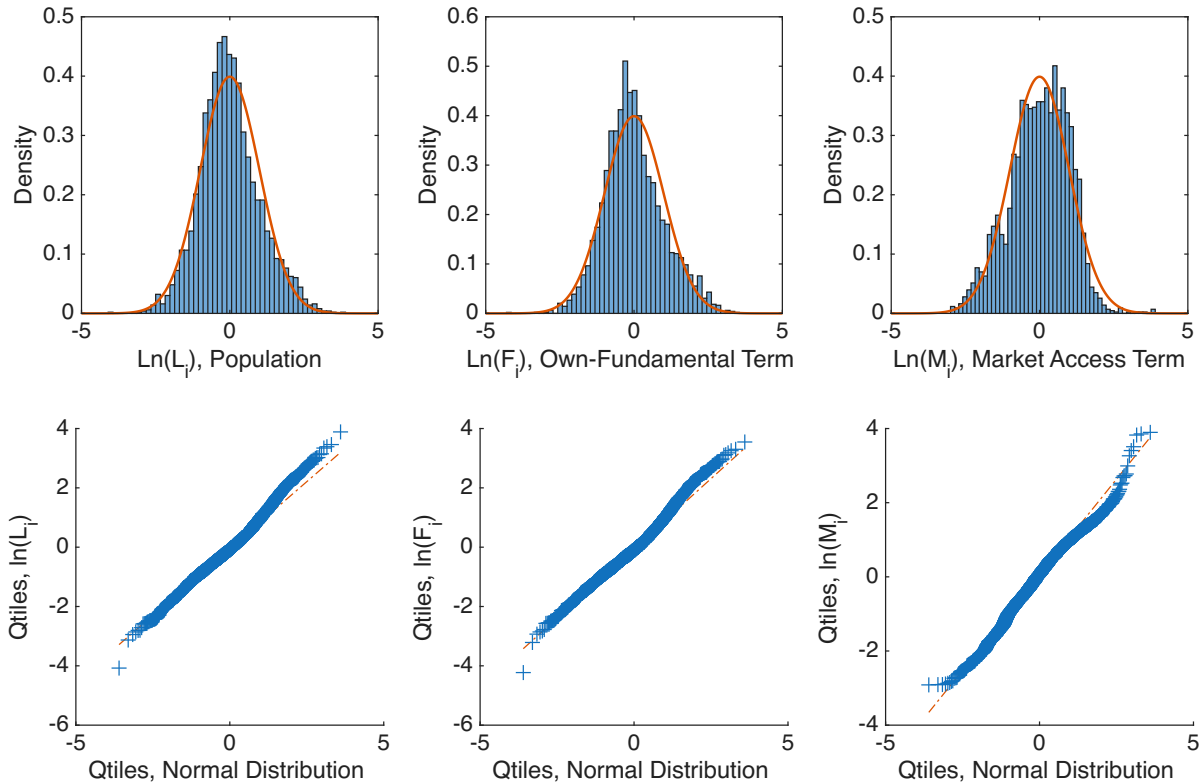
The distribution of county populations is shown in the left-hand column of Figure II, with both the density and QQ plot exhibiting a close fit to a lognormal distribution. The recovered own-fundamental terms  $F_i$ , plotted in the middle column, are also strikingly lognormal. The recovered empirical market access terms  $M_i$  are also lognormally distributed. These results provide empirical support for our decision to model fundamentals as lognormal and verify that our theoretical result regarding the distribution of market access holds in the data.

## 4.2 Simulation of the Population Distribution

We next simulate the model to investigate the robustness of our asymptotic theoretical results in a finite setting. We draw parameter values for this simulation from our model inversion and the literature. We reliably obtain lognormal population distributions and a “Zipf’s” coefficient near -1 as often identified in the literature in the log-rank, log-size regression. We use the simulation to explore how changes to the model parameters affect the observed population distribution, with particular attention to deviations in the estimated “Zipf’s” coefficient. We find that the changes we observe in simulation are able to rationalize variation in city-size distributions observed across countries in terms of differences in the benefits of agglomeration, costs from congestion, and trade costs between locations.

We simulate the model within a two-dimensional geography. Each location in the

**Figure II:** Populations, Recovered Fundamentals, and Resulting Market Access



*Notes:* The figure shows the distribution of population across US counties along with the distributions of the recovered own-fundamental terms  $F_i$  and the market access terms  $M_i$ . All of the distributions have been normalized for comparison against a standard normal distribution. The distribution of the recovered terms appear lognormal, as predicted by the theory.

**Table I:** Parameters used for simulation

Parameters		Value	Source
Agglomeration	$\alpha$	0.03	Literature
Congestion	$\beta$	-1/3	Literature
Elasticity of Substitution	$\sigma$	5	Literature
Trade cost increase with distance	$\tau_{ij} = e^{\delta_{TC} d_{ij}}$	$\delta_{TC} = 1.204$	Inversion
Lognormal fundamentals $A_i, U_i$	$\sim \exp N(0, \sigma)$	$\sigma = 0.5$	Inversion
Correlation of $A_i, U_i$	$\rho_{AU}$	0.39	Inversion
Spatial correlation in $A_i, A_j$ and $U_i, U_j$	$\rho_{ij} = e^{\delta_{corr} d_{ij}}$	$\delta_{corr} = -20.932$	Inversion

model is a place that can host a settlement.<sup>21</sup> We define the most populous 5% of locations as “cities” within the model, to demonstrate that the tail behavior of the resulting population distribution mirrors the appearance of a power law in empirical city size distributions.

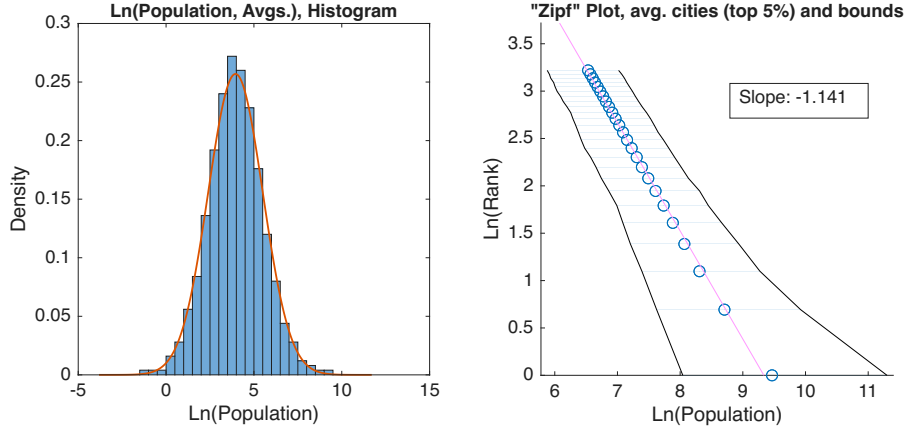
We take model parameters from the literature and from our empirical inversion. Our parameters are recorded in Table I. Key model parameters  $\alpha$ ,  $\beta$ , and  $\sigma$  are drawn from the literature and match those used in our model inversion. We create a 100-by-100 grid that we populate with 500 settlements, with the width of the grid normalized to 1. We also create a “buffer” region surrounding the central geography that we fill with an equal density of additional settlements, in order to limit the impact of border effects on market access. We distribute these settlements randomly over the full geography to create a “dartboard” geography, ensuring dispersion in distances between locations. The dispersion in geographic distances from the dartboard geography provides both variation in (geographic) trade costs  $\tau_{ij} = e^{\delta_{TC} d_{ij}}$ . The geographic distances generated by the dartboard approach also allow us to match the spatial correlation fundamentals between different locations. We parameterize  $\delta_{TC}$  based on our trade costs estimation. We model the spatial correlation in fundamentals as declining exponentially with distance such that  $\rho_{ij} = e^{\delta_{corr} d_{ij}}$ , and use the observed spatial correlation in fundamentals from our inversion to parameterize  $\delta_{corr}$ . We take a lognormal realization for  $A_i$  and  $U_i$  for each settlement, matching the variance of these draws to the realizations from our model inversion exercise after normalizing the mean value to 1. The correlation between  $A_i$  and  $U_i$  within each location is also set to match the correlation from our model inversion. Further details on the parameterization are given in Appendix E.

We demonstrate the robustness of the lognormal population distribution by performing 1000 simulations, each time drawing a new random geography and fundamentals.

---

<sup>21</sup>This interpretation matches that in Redding and Rossi-Hansberg (2017), which frames locations as regions that can potentially hold a single settlement.

**Figure III:** Smoothed Output Over 1000 MC Simulations



*Notes:* The population distribution resulting from numerical simulation of the model is in the left panel. The city size distribution is in the right panel. The slope in the left panel represents the slope taken over the average of log(pop) at each rank over 1000 simulations, and the bounds contain 90% of the realized populations at each rank of the distribution.

**Table II:** Normality Tests

	Kolmogorov-Smirnov	Lilliefors	Jarque-Bera
Rejected at 1%	0.001	0.051	0.327
Rejected at 5%	0.003	0.185	0.510

*Notes:* Table shows the share of tests for a normal distribution rejected for the log equilibrium population of 1000 simulations. The Jarque-Bera test rejects at a higher rate than the Kolmogorov-Smirnov and Lilliefors tests, which may be due to its inappropriateness for use on correlated data (Bai and Ng 2005).

Figure III displays smoothed results over 1000 simulations of the model.<sup>22</sup> The (log) rank-size regression on the smoothed distribution delivers a slope of -1.14. It is interesting that the model, using standard parameters from the literature and our inversion, closely approximates the Zipf's Law coefficient of -1. While interesting, as the tail of a lognormal distribution this coefficient is sensitive to the scale of the simulation and the truncation point as discussed in Section 2 and Supplemental Appendix B and should not be taken as a meaningful feature of the simulation. The  $\sigma_{LN}$  parameter associated with the resulting log population distribution is  $\hat{\sigma}_{LN} = 1.536$ , very close to the value  $\sigma_{LN} = 1.75$  identified by Eeckhout (2004) on U.S. data.

<sup>22</sup>The log of population is averaged at each rank of the distribution (1 to 1000) over the 1000 simulations. Results are similar when averaging the population and taking the log, or when considering the median population.

**Table III:** Simulated changes in distribution

	$\frac{\partial \theta_1}{\partial \alpha}$	$\frac{\partial \theta_1}{\partial \beta}$	$\frac{\partial \theta_1}{\partial \delta_{TC}}$
Sign of change	+	+	+

*Notes:* Direction of the change in slope coefficient in the (log) rank-size regression for changes in  $\alpha$ ,  $\beta$ , and  $\delta_{TC}$ , holding other parameters constant. “+” means the estimated slope (which is negative by construction) has become flatter. This implies that the largest cities are relatively bigger than smaller cities. Note that  $\beta < 0$ , so an increase in  $\beta$  means a decrease in congestion. The signs are from a regression of the parameters on the estimated coefficients (discussed in Supplemental Appendix E.2)

We test each of the 1000 simulated population distributions against the null hypothesis that the logged population distribution is normally distributed using the Kolmogorov-Smirnov, Lilliefors, and Jarque-Bera tests. The results of these tests are given in Table II. The Kolmogorov-Smirnov test rarely rejects the normality of the log population distribution at either level of significance. The Lilliefors correction, which is more sensitive to deviations in the tails, rejects at a higher rate but only rejects the normality of a small share of the resulting log population distributions at the 1% level. The deviations in the tails may be due to simulation on a finite grid, which results in central regions having systematically better market access than peripheral areas even with the buffer area. The smoothed population distribution in Figure III exhibits a degree of kurtosis, with slightly heavy tails. The Jarque-Bera test rejects the normality of the simulated population distribution at a higher rate, but this test is not appropriate for correlated data (like the spatial data simulated here) as noted in Bai and Ng (2005). These results suggest the need for future work developing better tests for the empirical distributions of correlated data.

We next simulate the comparative statics of the estimated power law coefficient for the city size distribution, testing its sensitivity to changes in model parameters. Changing parameters alters the estimated coefficient of the log rank-size regression, which we denote  $\theta_1$  as in Equation 1. We perform 100 simulations for each of 150 combinations of parameters.<sup>23</sup> A summary of the signs of changes (estimated by a regression given in Supplemental Appendix E.2) is provided in Table III.

The comparative statics of our model demonstrate changes in the estimated power law coefficient in line with empirical evidence. Increasing the benefits of agglomeration by raising  $\alpha > 0$  results in a more unequal city size distribution (greater dispersion, or a flatter slope) and increasing local congestion costs by reducing  $\beta < 0$  results in a more equal

---

<sup>23</sup>We simulate for 5 values of  $\alpha$ , 6 values of  $\beta$ , and 5 values of  $\delta_{TC}$  given in Supplemental Appendix E.2. The geography has the same dimensions as our baseline simulations but to reduce the computational intensity of the simulations we fix the randomly drawn dartboard geography for each combination of parameter values and only draw a new set of fundamentals for each simulation on the fixed geography.

distribution (less dispersion, or a steeper slope). Increasing trade costs by increasing the rate at which these costs grow with distance,  $\delta_{TC} > 0$ , likewise results in a more unequal city size distribution. In many developing countries, the city size distributions are highly unequal, generating the flatter slopes in the log-log regression documented in Duben and Krause (2021). These unequal city size distributions could be attributable to high domestic transportation costs, which are often substantially higher in developing than in developed countries. Atkin and Donaldson (2015) estimate that domestic trade costs are roughly four to five times higher in Nigeria and Ethiopia than in the U.S., in line with the empirical evidence documented in Teravaninthorn and Gaël (2009). These high domestic trade costs could contribute to the phenomenon of very large metropolises relative to secondary cities (“primate cities”) within the developing world. Additionally, the flattening slope in the U.S. in recent decades, documented in Gabaix and Ioannides (2004), could be a result of increased agglomeration benefits in the modern services economy.

### 4.3 Gibrat’s Law

Allen and Arkolakis (2014) demonstrate that the population vector is scaled by changes in the aggregate population, but the relative populations over locations are not changed by changes in the total population. We now demonstrate that, based on this property, the equilibrium population distribution demonstrates proportional growth and satisfies Gibrat’s law in response to increases in the aggregate population  $\bar{L}$ . We can the matrix-form representation of Equation 17 as:

$$\tilde{\mathbf{h}} = \mathbf{J}[\tilde{\mathbf{h}}]^{\frac{\gamma_2}{\gamma_1}}$$

where  $\tilde{h}_{i'} = h_{i'} \bar{W}^{\frac{\sigma-1}{1-\gamma_2}}$ , the notation  $[.]^a$  indicates raising each element of the vector to the power  $a$ .<sup>24</sup> As this relationship must hold for any level of  $\bar{L}$ , changing  $\bar{L}$  does not impact the resulting population distribution even as it impacts welfare ( $\bar{W}$ , which is the same across all locations). That is, a percentage increase in the overall population will result in each location experiencing population growth of the same percentage. As a result, population growth rates will be unrelated to initial population and Gibrat’s law will hold within the equilibrium of this model.

This is a key difference between our explanation for observed population distributions based on locational fundamentals and trade and the prior literature on random growth models. Rather than being the force creating the equilibrium distribution, random growth

---

<sup>24</sup>The matrix  $\mathbf{J}$  is given in Supplemental Appendix A.4 along with the full expression of the matrix form of Equation 17 in Appendix Equation A.7

is a feature of an equilibrium based on the underlying characteristics of place and trade. This view is supported by the absence of Gibrat's law in systems that are in transition or have suffered disequilibrating shocks (Desmet and Rappaport 2017; Davis and Weinstein 2002, 2008).

## 5 Conclusion

The power law-like distribution of city populations is a striking empirical regularity that holds across countries and over millennia. In this paper, we demonstrate that a broad class of economic geography models generate these characteristic population distributions when modeled with a realistic geography. We integrate insights from economic geography theory regarding the importance of both the qualities of a location and its market access for its population into the extensive literature on power law-like population distributions and Zipf's Law. An inversion of the model on U.S. data supports our proposed mechanisms. Viewing population distributions as arising naturally in response to favorable geography and trade access provides a simple explanation for the emergence of the distinctive city size distribution. This explanation is consistent with the persistence of human settlements, the recovery of cities from disasters, and the random growth of cities in equilibrium.

## References

- Adão, R., A. Costinot, and D. Donaldson (2023). Putting Quantitative Models to the Test: An Application to Trump's Trade War. Technical report, National Bureau of Economic Research.
- Alix-Garcia, J. and E. A. Sellars (2020). Locational fundamentals, trade, and the changing urban landscape of Mexico. *Journal of Urban Economics* 116, 103213.
- Allen, T. and C. Arkolakis (2014). Trade and the Topography of the Spatial Economy. *Quarterly Journal of Economics* 129(3), 1085–1140.
- Atkin, D. and D. Donaldson (2015). Who is Getting Globalized? The Size and Implications of Intranational Trade Costs. Working paper.
- Auerbach, F. (1913). Das Gesetz der Bevölkerungskonzentration. *Petermann's Geographische Mitteilungen*.
- Auerbach, F. and A. Ciccone (2023). The Law of Population Concentration. *Envmt. and Planning B: Urban Analytics and City Sc.* 50(2), 290–298.
- Bai, J. and S. Ng (2005). Tests for Skewness, Kurtosis, and Normality for Time Series Data. *Journal of Business and Economic Statistics* 23(1), 49–60.
- Bailey, M., R. Cao, T. Kuchler, J. Stroebel, and A. Wong (2018, August). Social connectedness: Measurement, determinants, and effects. *Journal of Economic Perspectives* 32(3), 259–80.
- Behrens, K. and F. Robert-Nicoud (2015). Agglomeration Theory with Heterogenous Agents. *Handbook in Regional and Urban Economics Ch.* 5.
- Blank, A. and S. Solomon (2000). Power laws in cities population, financial markets and internet sites (scaling in systems with a variable number of components). *Physica A: Statistical Mechanics and its Applications* 287(1), 279–288.
- Bosker, M. and E. Buringh (2017). City seeds: Geography and the origins of the european city system. *Journal of Urban Economics* 98, 139–157.
- Bradley, R. C. (2005). Basic Properties of Strong Mixing Conditions. A Survey and Some Open Questions. *Probability Surveys* 2(N.A.).
- Brakman, S., H. Garretsen, and M. Schramm (2004). The strategic bombing of German cities during World War II and its impact on city growth. *Journal of Economic Geography* 4(2), 201–218.
- Brakman, S., H. Garretsen, C. Van Marrewijk, and M. Van Den Berg (1999). The Return of Zipf: Towards a Further Understanding of the Rank-Size Distribution. *Journal of Regional Science* 39(1), 183–213.
- Combes, P.-P., G. Duranton, and L. Gobillon (2008). Spatial wage disparities: Sorting matters! *Journal of Urban Economics* 63(2), 723–742.
- Combes, P.-P., G. Duranton, and L. Gobillon (2019). The Costs of Agglomeration: House and Land Prices in French Cities . *Review of Economic Studies*, 1556–1589.
- Combes, P.-P. and L. Gobillon (2015). Chapter 5 - The Empirics of Agglomeration Economies. In *Handbook of Regional and Urban Economics*, Volume 5, pp. 247–348. Elsevier.
- Cuberes, D., K. Desmet, and J. Rappaport (2021). Urban growth shadows. *Journal of Urban Economics* 123, 103334.
- Córdoba, J.-C. (2008). On the distribution of city sizes. *Journal of Urban Economics* 63(1),

- 177–197.
- Davis, D. R. and D. E. Weinstein (2002). Bones, Bombs, and Break Points: The Geography of Economic Activity. *American Economic Review* 92(5), 1269–1289.
- Davis, D. R. and D. E. Weinstein (2008). A Search for Multiple Equilibria in Urban Industrial Structure. *Journal of Regional Science* 48(1), 29–65.
- Davis, M. A. and F. Ortalo-Magné (2011). Household expenditures, wages, rents. *Review of Economic Dynamics* 14(2), 248–261.
- Desmet, K. and J. Rappaport (2017). The settlement of the United States, 1800–2000: The long transition towards Gibrat's law. *Journal of Urban Economics* 98, 50–68.
- Duben, C. and M. Krause (2021). Population, light, and the size distribution of cities. *Journal of Regional Science*, 189–211.
- Eeckhout, J. (2004). Gibrat's Law for (All) Cities. *American Economic Review*, 1429–1451.
- Eeckhout, J. (2009). Gibrat's Law for (All) Cities: Reply. *American Economic Review* 99(4), 1676–83.
- Frigg, R., J. Berkovitz, and F. Kronz (2020). The Ergodic Hierarchy. In E. N. Zalta (Ed.), *The Stanford Encyclopedia of Philosophy* (Fall 2020 ed.). Metaphysics Research Lab, Stanford University.
- Fujita, M., P. Krugman, and A. J. Venables (1999). *The Spatial Economy: Cities, Regions, and International Trade*. The MIT Press.
- Gabaix, X. (1999a). Zipf's Law and the Growth of Cities. *The American Economic Review* 89(2), 129–132.
- Gabaix, X. (1999b). Zipf's Law for Cities: An Explanation. *The Quarterly Journal of Economics*.
- Gabaix, X. (2009). Power Laws in Economics and Finance. *Annual Review of Economics* 1(1), 255–294.
- Gabaix, X. and Y. M. Ioannides (2004). The Evolution of City Size Distributions. In: *Handbook of Regional and Urban Economics*, 2341–2378.
- Gibrat, R. (1931). *Les inégalités économiques*. Paris: Librairie du Recueil Sirey.
- Head, K. and T. Mayer (2009). Illusory border effects: Distance mismeasurement inflates estimates of home bias in trade. In *The Gravity Model in International Trade: Advances and Applications*. Cambridge University Press.
- Head, K. and T. Mayer (2011). Gravity, market potential and economic development. *Journal of Economic Geography* 11.
- Helpman, E. (1998). The Size of Regions. *Topics in Public Economics: Theoretical and Applied Analysis*, 33–54.
- Henderson, J. V., T. Squires, A. Storeygard, and D. Weil (2018). The Global Distribution of Economic Activity: Nature, History, and the Role of Trade. *The Quarterly Journal of Economics* 133(1), 357–406.
- Herrndorf, N. (1984). A Functional Central Limit Theorem for Weakly Dependent Sequences of Random Variables. *The Annals of Probability* 12(1), 141 – 153.
- Holmes, T. J. and S. Lee (2010). Cities as Six-by-six-mile Squares: Zipf's Law? In *Agglomeration Economics*. NBER.
- Hsu, W.-T. (2012). Central place theory and city size distribution. *The Economic Journal* 122(563), 903–932.
- Johnson, N., R. Jedwab, and M. Koyama (2019). Pandemics, Places, and Populations:

- Evidence from the Black Death. *Working Paper*.
- Krugman, P. (1991). Increasing returns and economic geography. *Journal of Political Economy* 99(3), 483–499.
- Krugman, P. (1996). *The Self-Organizing Economy*. Blackwell.
- Lee, S. and Q. Li (2013). Uneven landscapes and city size distributions. *Journal of Urban Economics* 78, 19–29.
- Malevergne, Y., V. Pisarenko, and D. Sornette (2011). Gibrat's Law for Cities: Uniformly Most Powerful Unbiased Test of the Pareto Against the Lognormal. *Physical Review*.
- Marlow, N. (1967). A Normal Limit Theorem for Power Sums of Independent Random Variables. *Bell System Technical Journal* 46(9), 2081–2089.
- Mori, T., T. E. Smith, and W.-T. Hsu (2020). Common power laws for cities and spatial fractal structures. *Proceedings of the National Academy of Sciences* 117(12), 6469–6475.
- Nordhaus, W. D. (2006). Geography and macroeconomics: New data and new findings. *Proceedings of the Natl Academy of Sciences* 103(10), 3510–3517.
- Nunn, N. and D. Puga (2012). Ruggedness: The Blessing of Bad Geography in Africa. *Review of Economics and Statistics* 94(1), 20–36.
- Rante, R., F. Trionfetti, and P. Verma (2024). The Size Distribution of Cities: Evidence from the Lab. working paper or preprint.
- Rappaport, J. and J. D. Sachs (2003). The United States as a Coastal Nation. *Journal of Economic Growth* 8(1), 5–46.
- Redding, S. and A. J. Venables (2004). Economic geography and international inequality. *Journal of International Economics* 62(1), 53–82.
- Redding, S. J. (2016). Goods trade, factor mobility and welfare. *Journal of International Economics*.
- Redding, S. J. and E. Rossi-Hansberg (2017). Quantitative Spatial Economics. *Annual Review of Economics*.
- Redding, S. J. and D. M. Sturm (2008, December). The costs of remoteness: Evidence from german division and reunification. *American Economic Review* 98(5), 1766–97.
- Rosenthal, S. S. and W. C. Strange (2004). Chapter 49 - Evidence on the Nature and Sources of Agglomeration Economies. In J. V. Henderson and J. Thisse (Eds.), *Cities and Geography*, Volume 4 of *Handbook of Regional and Urban Economics*, pp. 2119–2171. Elsevier.
- Rossi-Hansberg, E. and M. Wright (2007). Urban Structure and Growth. *The Review of Economic Studies*, 597–624.
- Rozenfeld, H. D., D. Rybski, X. Gabaix, and H. A. Makse (2011). The Area and Population of Cities: New Insights from a Different Perspective on Cities. *American Economic Review* 101(5), 2205–25.
- Simonovska, I. and M. E. Waugh (2014). The elasticity of trade: Estimates and evidence. *Journal of International Economics* 92(1), 34–50.
- Teravanithorn, S. and R. Gaël (2009). Transport Prices and Costs in Africa: A Review of the Main International Corridors. *World Bank Report*.
- Tobler, W. (1970). A Computer Movie Simulating Urban Growth in the Detroit Region. *Economic Geography* 46.
- Zipf, G. K. (1949). Human Behavior and the Principle of Least Effort. *Addison-Wesley Press*.

**SUPPLEMENTAL APPENDIX**  
for “Populations in Spatial Equilibrium”  
Matthew Easton and Patrick W. Farrell

This appendix includes proofs and additional material.

1. Discussion of Main Text Results and Proofs.
2. Pareto vs. Lognormal Evidence and Simulations
3. Exploring Attributes and Fundamentals
4. Model Inversion
5. Additional Details on Simulation

# A Discussion of Main Text Results and Proofs

## A.1 Algebra for “Pareto Form” of Lognormal PDF

The density function of a lognormal distribution is given by:

$$f(x) = \frac{1}{x\sigma\sqrt{2\pi}} \exp\left(-\frac{(\ln(x) - \mu)^2}{2\sigma^2}\right)$$

Expanding the square and grouping the  $\ln(x)$  terms yields:

$$f(x) = \frac{1}{x\sigma\sqrt{2\pi}} \exp\left(\ln\left(x^{\left(\frac{-\ln(x)+2\mu}{2\sigma^2}\right)}\right) - \frac{\mu^2}{2\sigma^2}\right)$$

Applying  $e^{\ln(a^b)} = a^b$  and combining with  $x^{-1}$ :

$$f(x) = \frac{1}{\sigma\sqrt{2\pi}} \exp\left(-\frac{\mu^2}{2\sigma^2}\right) x^{-\left(\frac{\ln(x)-2\mu}{2\sigma^2}\right)-1}$$

Writing the constant term  $\frac{1}{\sigma\sqrt{2\pi}}$  as  $\Gamma$ , the lognormal distribution can be written as:

$$f(x) = \Gamma x^{-\alpha(x)-1} \quad , \text{ where } \alpha(x) = \frac{\ln(x) - 2\mu}{2\sigma^2}$$

which is the same as Equation 3 in the main text. The representation of the lognormal PDF here appears in Malevergne et al. (2011), and is similar to that in Eeckhout (2009).

The lognormal distribution, while fitting the body of the population distribution well, provides somewhat worse fit compared to similar distributions with more parameters, such as the double Pareto lognormal. We focus on describing the full population distribution as lognormal for relative simplicity of analysis. More robust discussions of goodness-of-fit tests and alternative statistical descriptions of population distributions can be found in Giesen et al. (2010) and Ioannides and Skouras (2013).

## A.2 Discussion of Lemma 2 (Marlow 1967)

A demonstration of the apparent normality in both levels and logs of sum of positive random variables is included in the main text in Figure A.I, which shows the sums of lognormal ( $\exp(N(0, 1))$ ), truncated normal (a standard normal truncated at 0), and  $(0, 1]$  uniform random variables. The sums of these random variables converge to normal distributions, while the log of the sum also appears to follow a normal distribution.

Examples of sums over several positive random variables (lognormal, truncated normal, and uniform) are presented in Figure A.I, exhibiting the appearance of normality in both levels and logs for these sums.

The Marlow result is interesting, as it appears to imply that a sum of positive random variables can be viewed as approaching a lognormal or normal distribution for large  $N$ . However, if we are considering both the normal and lognormal approximations for a sum of positive random variables we can demonstrate convergence of the lognormal approximation to the equivalent normal approximation—that is, the lognormal and normal approximation will be identical in the limit. The following discussion draws on Mazmanyan et al. (2008).

For simplicity, consider an approximation of *i.i.d.* positive random variables with mean  $m$  and variance  $s^2$ . The normal approximation will have parameters  $\mu_N = nm = M$  and  $\sigma_N^2 = ns^2$ . We will now define the parameters for the lognormal approximation of the sum.

First, define the coefficient of variation as

$$C_v = \frac{\sqrt{ns^2}}{nm} = \frac{\sqrt{ns}}{nm} \quad (\text{A.1})$$

As  $n$  grows large,  $C_v \rightarrow 0$ .

The parameters  $\mu_X$  and  $\sigma_X$  of the lognormal approximation can be found by

$$\sigma_X^2 = \ln(1 + C_v^2) \quad (\text{A.2})$$

$$\mu_X = \ln(nm) - \frac{\sigma_X^2}{2} \quad (\text{A.3})$$

As  $C_v \rightarrow 0$  when  $n \rightarrow \infty$ , Equation (25) gives that as  $n \rightarrow \infty$ :

$$\sigma_X^2 \rightarrow C_v^2 \quad , \text{so} \quad \sigma_X \rightarrow C_v \quad , \text{and} \quad \sigma_X \rightarrow 0 \quad (\text{A.4})$$

Now we demonstrate that the lognormal approximation converges to the expected normal. As, for some  $m$ ,  $P(||x - M|| > \epsilon | n \geq m) = 0$ , so  $\frac{x}{M} \rightarrow_{a.s.} 1$ . We can write  $\frac{x}{M} \cdot \sigma_X \rightarrow \frac{\sqrt{ns}}{nm}$ , and so  $x\sigma_X \rightarrow \sqrt{ns} = \sigma_N$ . This means  $\frac{1}{x\sigma_X\sqrt{2\pi}} \rightarrow \frac{1}{\sigma_N\sqrt{2\pi}}$ .

Similarly,  $x = \frac{xM}{M}$ , so  $\ln(x) = \ln(M) + \ln(\frac{x}{M})$ . As  $\frac{x}{M} \rightarrow 1$ , so  $\ln(\frac{x}{M}) \rightarrow \frac{x-M}{M}$ . As  $\mu_X = \ln(M) - \frac{\sigma_X^2}{2}$ , and  $\sigma_X \rightarrow C_v \rightarrow 0$ , and  $M = \mu_N$  then we have

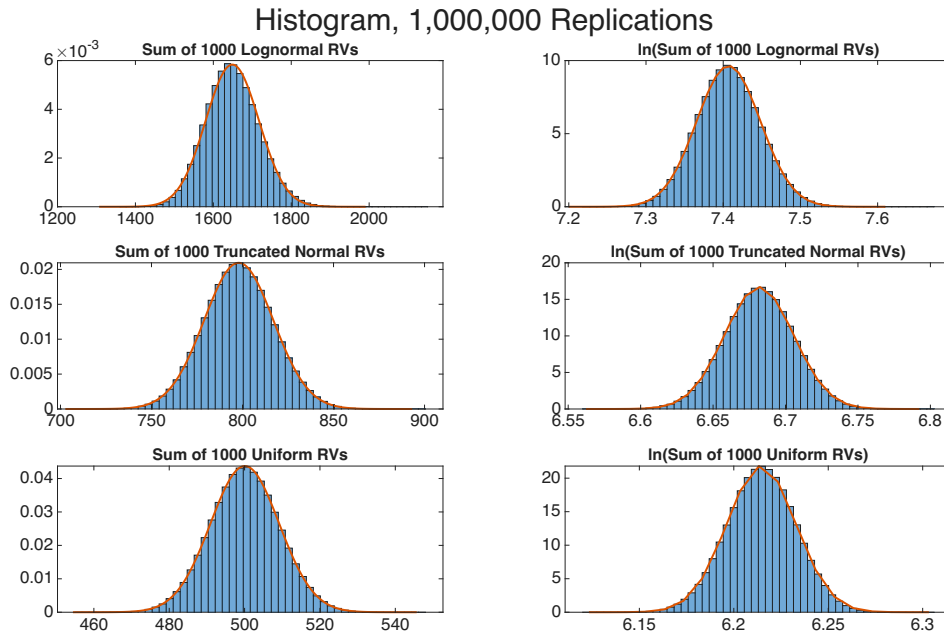
$$\frac{\ln(x) - \mu_x}{\sigma_X} \rightarrow \frac{\ln(M) + (\frac{x-M}{M}) - \ln(M)}{\sigma_X} = \frac{x - M}{M\sigma_X} \rightarrow \frac{x - M}{M \cdot C_v} = \frac{x - \mu_X}{\sigma_N} \quad (\text{A.5})$$

So we have shown, as  $n \rightarrow \infty$ ,

$$f(x) = \frac{1}{x\sigma_X\sqrt{2\pi}} e^{-\frac{1}{2}\left(\frac{\ln(x)-\mu_X}{\sigma_X}\right)^2} \rightarrow \frac{1}{\sigma_N\sqrt{2\pi}} e^{-\frac{1}{2}\left(\frac{x-\mu_N}{\sigma_N}\right)^2} \quad (\text{A.6})$$

So as  $n$  increases, the lognormal approximation to the sum approaches the normal approximation.

**Figure A.I:** Sums of Positive Random Variables, Various Distributions



*Notes:* Histograms show 1,000,000 replications. The random variables in the first row are drawn from a lognormal distribution with parameters  $\mu_{LN} = 0, \sigma_{LN} = 1$ , the middle row from a truncated normal distribution with parameters  $\mu_{TN}, \sigma_{TN} = 0$  and minimum value  $\alpha = 0.001$ , and the bottom row from a uniform distribution on  $(0, 1]$ . The red overlaid line represents a normal distribution with the same mean and standard deviation as the underlying sums in each panel. The sums appear distributed normally in both levels (column 1) and in logs (column 2), as implied by Lemma 1.

### A.3 Additional Proofs

A remaining point is the  $\alpha$ -mixing of the population distribution itself. We want to ensure that the distribution is such that the full distribution is realized—we further require that populations are not too correlated across locations. While we have proven that the distribution of the population in each  $i$  approaches a lognormal, we did not formally rule out the case where the population is perfectly correlated such that the PDF of the realized population distribution appears degenerate.

The mixing definition applied in the main text applies to sequences. To consider the mixing of the population, we now require a shift from considering the mixing properties of points or summations defined over sequences for individual locations to considering the mixing properties of the random variables across the full plane. Population is defined on a plane and is a random field, a generalization of random sequences to a multidimensional space. A random field is a collection of  $X$ -valued random variables indexed by elements in a topological space  $T$ .

The following definition of  $\alpha$ -mixing for random fields is used when considering  $\alpha$ -mixing of the population across the two-dimensional geography.

**Definition 2,  $\alpha$ -mixing (fields):** Suppose  $\{X_i\}, i \in \mathbb{Z}^2$  is a stationary random field where each  $X_i$  is drawn from a common distribution. For disjoint sets  $S, T$ , define the  $\sigma$ -fields:

$$\mathcal{F}_S := \sigma(X_s, s \in S), \mathcal{F}_T := \sigma(X_t, t \in T).$$

The notation  $\sigma(\dots)$  means the  $\sigma$ -field  $\subset \mathcal{F}$  generated by  $(\dots)$ . Define:

$$\alpha(S, T) = \sup_{A \in \mathcal{F}_S, B \in \mathcal{F}_T} |\mathbb{P}(A \cap B) - \mathbb{P}(A)\mathbb{P}(B)|.$$

Define  $dist(S, T) = \inf_{s \in S, t \in T} \|s - t\|$ , where  $\|\cdot\|$  denotes the Euclidean norm. For each  $k \geq 1$  and  $u, v \in \mathbb{R}_{++}$ , define:

$$\alpha(k; u, v) := \sup_{S, T} \alpha(S, T),$$

where the supremum is taken over all disjoint subsets  $S, T$  with  $|S| \leq u, |T| \leq v$  such that  $dist(S, T) \geq k$ . The random field  $\{X_i\}$  is said to be “strongly mixing” (or “ $\alpha$ -mixing”) if  $\alpha(k; \infty, \infty) \rightarrow 0$  as  $k \rightarrow \infty$ .

The definition above is drawn from Doukhan (1994) and Bradley (1993), both of which also include further discussion and additional mixing concepts for fields. The key distinction from the definition for sequences introduced earlier is the need to incorporate a

concept of distance, which previously was summarized by the indices when considering  $\alpha$ -mixing of a sequence.

Under certain conditions we can show that the population will be  $\alpha$ -mixing, which will ensure that populations will be asymptotically independent across space. The restrictions necessary to establish  $\alpha$ -mixing are strict, and  $\alpha$ -mixing is not itself a necessary condition for the ergodicity of the population distribution as  $\alpha$ -mixing is a stronger concept that implies ergodicity (Frigg et al. 2020).

To ensure this, we introduce a Lemma that generalizes  $\alpha$ -mixing results for sequences.

**Lemma 3:** Suppose that for each  $n = 1, 2, 3, \dots$ ,  $X^{(n)} := (X_i^{(n)}, i \in \mathbb{Z}^2)$  is a (not necessarily stationary) field of random variables. Suppose these fields  $X^{(n)}$ ,  $n = 1, 2, 3, \dots$  are independent of each other. Suppose that for each  $i \in \mathbb{Z}^2$ ,  $h_i : \mathbb{R} \times \mathbb{R} \times \mathbb{R} \times \dots \rightarrow \mathbb{R}$  is a Borel function. Define the field  $X := (X_i, i \in \mathbb{Z}^2)$  of random variables by  $X_i := h_i(X_i^{(1)}, X_i^{(2)}, X_i^{(3)}, \dots)$ ,  $i \in \mathbb{Z}^2$ . Then for each  $k \geq 1$ ,  $\alpha_X(k, \infty, \infty) \leq \sum_{n=1}^{\infty} \alpha_{X^{(n)}}(k, \infty, \infty)$ , where  $\alpha_Z$  indicates the mixing coefficient for field  $Z$ .

The proof of Lemma 3 is stated below.

**Proof:** First, we want to show that  $\alpha$ -mixing is preserved over measurable transformations of  $\alpha$ -mixing random fields, and then we want to show that combinations of  $\alpha$ -mixing random fields are also mixing. For brevity, we write  $\alpha(k)$  in place of  $\alpha(k; \infty, \infty)$ .

1. Define the field  $\{\bar{D}_i\}$  such that for all  $i \in \mathbb{Z}^2$ ,  $\bar{D}_i = j(D_i^{(1)}, D_i^{(2)}, D_i^{(3)}, \dots)$ , where  $j(\cdot)$  is a measurable mapping that takes the field  $\{D_i\}$ , which is an  $n$ -tuple of random variables for each  $i \in \mathbb{Z}^2$ , as input. The field  $\{D_i\}$  is  $\alpha$ -mixing with respect to distance  $k$ . We want to show that the field  $\{\bar{D}_i\}$  will be mixing as well. First note that

$$\begin{aligned} \mathbb{P}(\bar{D}_{s \in S} \in A, \bar{D}_{t \in T} \in B) &= \mathbb{P}\left((D_{s \in S}^{(1)}, D_{s \in S}^{(2)}, D_{s \in S}^{(3)}, \dots) \in j^{-1}(A), \right. \\ &\quad \left.(D_{t \in T}^{(1)}, D_{t \in T}^{(2)}, D_{t \in T}^{(3)}, \dots) \in j^{-1}(B)\right) \end{aligned}$$

And so,

$$\begin{aligned} \alpha_{\bar{D}}(k) &= \sup_{A, B} |\mathbb{P}(\bar{D}_{s \in S*} \in A, \bar{D}_{t \in T*} \in B) \\ &\quad - \mathbb{P}(\bar{D}_{s \in S*} \in A) \mathbb{P}(\bar{D}_{t \in T*} \in B)| \\ &= \sup_{A, B} |\mathbb{P}\left((D_{s \in S*}^{(1)}, \dots) \in j^{-1}(A), (D_{t \in T*}^{(1)}, \dots) \in j^{-1}(B)\right) \\ &\quad - \mathbb{P}\left((D_{s \in S*}^{(1)}, \dots) \in j^{-1}(A)\right) \mathbb{P}\left((D_{t \in T*}^{(1)}, \dots) \in j^{-1}(B)\right)| \\ &\leq \alpha_D(k), \end{aligned}$$

as  $\alpha_D(k)$  is defined as the supremum over sets  $S, T$ , not the fixed  $S^*, T^*$  that correspond to  $\{\bar{D}_i\}$ . As  $\alpha_D(k) \rightarrow 0$  as  $k \rightarrow \infty$ , then  $\alpha_{\bar{D}}(k) \rightarrow 0$  as well and so  $\{\bar{D}_i\}$  is  $\alpha$ -mixing.

2. We now show that given two independent stationary random fields  $\{Y_i\}, \{Z_i\}$  where  $i \in \mathbb{Z}^2$  which are  $\alpha$ -mixing with respect to distance  $k$ , the bivariate field  $\{X_i\}$  where  $X_i = (Y_i, Z_i)$  is also mixing.

Define  $I$ :

$$\begin{aligned} I &= |\mathbb{P}(X_{s \in S} \in A, X_{t \in T} \in B) - \mathbb{P}(X_{s \in S} \in A)\mathbb{P}(X_{t \in T} \in B)| \\ &= |\mathbb{P}((Y_{s \in S}, Z_{s \in S}) \in A, (Y_{t \in T}, Z_{t \in T}) \in B) \\ &\quad - \mathbb{P}((Y_{s \in S}, Z_{s \in S}) \in A)\mathbb{P}((Y_{t \in T}, Z_{t \in T}) \in B)| \end{aligned}$$

Define

$$\begin{aligned} f(Z_{s \in S}, Z_{s \in T}) &= \mathbb{P}((Y_{s \in S}, Z_{s \in S}) \in A, (Y_{t \in T}, Z_{t \in T}) \in B) \\ g(Z_{s \in S}) &= \mathbb{P}((Y_{s \in S}, Z_{s \in S}) \in A) \\ h(Z_{t \in T}) &= \mathbb{P}((Y_{t \in T}, Z_{t \in T}) \in B) \end{aligned}$$

Substituting in and taking expectations,

$$I = |\mathbb{E}[f(Z_{s \in S}, Z_{s \in T})] - \mathbb{E}[g(Z_{s \in S})h(Z_{t \in T})]|$$

Add and subtract  $\mathbb{E}[g(Z_{s \in S})]\mathbb{E}[h(Z_{t \in T})]$ :

$$\begin{aligned} &= |\mathbb{E}[f(Z_{s \in S}, Z_{s \in T})] - \mathbb{E}[g(Z_{s \in S})]\mathbb{E}[h(Z_{t \in T})] \\ &\quad + \mathbb{E}[g(Z_{s \in S})]\mathbb{E}[h(Z_{t \in T})] - \mathbb{E}[g(Z_{s \in S})h(Z_{t \in T})]| \end{aligned}$$

Re-arrange and, using the  $|\cdot|$ ,

$$\begin{aligned} &= |\mathbb{E}[f(Z_{s \in S}, Z_{s \in T})] - \mathbb{E}[g(Z_{s \in S})]\mathbb{E}[h(Z_{t \in T})] \\ &\quad - (\mathbb{E}[g(Z_{s \in S})h(Z_{t \in T})] - \mathbb{E}[g(Z_{s \in S})]\mathbb{E}[h(Z_{t \in T})])| \\ &\leq \underbrace{|\mathbb{E}[f(Z_{s \in S}, Z_{s \in T})] - \mathbb{E}[g(Z_{s \in S})]\mathbb{E}[h(Z_{t \in T})]|}_{II} \\ &\quad + \underbrace{|\mathbb{E}[g(Z_{s \in S})h(Z_{t \in T})] - \mathbb{E}[g(Z_{s \in S})]\mathbb{E}[h(Z_{t \in T})]|}_{III} \end{aligned}$$

Begin with  $II$ , where we use independence of  $Y, Z$  and mixing of  $Y$  to show

$$\begin{aligned}
II &= |\mathbb{E}[f(Z_{s \in S}, Z_{s \in T})] - \mathbb{E}[g(Z_{s \in S})\mathbb{E}h(Z_{t \in T})]| \\
&= |\mathbb{E}[\mathbb{P}((Y_{s \in S}, Z_{s \in S}) \in A, (Y_{t \in T}, Z_{t \in T}) \in B)] \\
&\quad - \mathbb{E}[\mathbb{P}((Y_{s \in S}, Z_{s \in S}) \in A)]\mathbb{E}[\mathbb{P}((Y_{t \in T}, Z_{t \in T}) \in B)]| \\
&= |\mathbb{E}[\mathbb{P}((Y_{s \in S}, Z_{s \in S}) \in A, (Y_{t \in T}, Z_{t \in T}) \in B | Z_{s \in S} = z_{s \in S}, Z_{t \in T} = z_{t \in T})] \\
&\quad - \mathbb{E}[\mathbb{P}((Y_{s \in S}, Z_{s \in S}) \in A | Z_{s \in S} = z_{s \in S})]\mathbb{E}[\mathbb{P}((Y_{t \in T}, Z_{t \in T}) \in B | Z_{t \in T} = z_{t \in T})]| \\
&= |\mathbb{P}(Y_{s \in S} \in A, Y_{t \in T} \in B) - \mathbb{P}(Y_{s \in S} \in A)\mathbb{P}(Y_{t \in T} \in B)|
\end{aligned}$$

Taking the supremum over  $A, B$ , we have

$$II \leq \alpha_Y(S, T)$$

Now consider  $III$ :

$$\begin{aligned}
III &= |\mathbb{E}[g(Z_{s \in S})h(Z_{t \in T})] - \mathbb{E}[g(Z_{s \in S})]\mathbb{E}[h(Z_{t \in T})]| \\
&= |Cov(g(Z_{s \in S}), h(Z_{t \in T}))|
\end{aligned}$$

Note that  $\|g(Z_{s \in S})\|_\infty, \|h(Z_{t \in T})\|_\infty \leq 1$ . By Lemma 3.1 of Doukhan (1994) and the  $\alpha$ -mixing of  $\{Z_t\}$  we have

$$III \leq 4\alpha_Z(S, T)$$

And so, putting together the above and, taking the supremum over  $A, B$ :

$$\alpha_X(S, T) \leq \alpha_Y(S, T) + 4\alpha_Z(S, T)$$

Taking the supremum again over all  $S, T$  such that  $dist(S, T) \geq k$ , we find

$$\alpha_X(k) \leq \alpha_Y(k) + 4\alpha_Z(k)$$

And, as we know  $\alpha_Y(k), \alpha_Z(k) \rightarrow 0$  as  $k \rightarrow \infty$ , we have  $\alpha_X(k) \rightarrow 0$  as  $k \rightarrow \infty$  and so the field  $\{X_i\}$  is mixing with respect to distance  $k$ .

Combining the results of Parts 1 and 2 establishes the result. ■

The proof extends the result for  $\alpha$ -mixing sequences from Bradley (2005) Theorem 5.2 to  $\alpha$ -mixing fields in two dimensions.

Lemma 3 states that measurable transformations and combinations of  $\alpha$ -mixing fields are also  $\alpha$ -mixing. If our geography was one-dimensional, such as a circle or line, the equivalent statement is given by Theorem 5.2 of Bradley (2005) which establishes that  $\alpha$ -mixing is maintained over measurable transformations and over combinations of independent  $\alpha$ -mixing random sequences. As our geography is defined in two dimensions (to reflect a realistic geography), our Lemma 3 extends Theorem 5.2 of Bradley (2005) to two dimensions.

We assume that the sequences  $\{A_i\}$  and  $\{U_i\}$  are  $\alpha$ -mixing with respect to distance to reflect the patterns of correlation in geographic attributes across space.<sup>25</sup> This assumption captures the potential similarity of nearby locations and how this similarity vanishes with increasing distance, and is consistent with the argument for  $\alpha$ -mixing of the elements of the market access summation in the prior section.<sup>26</sup>

**Proposition 4:** *If  $\{A_i\}$  and  $\{U_i\}$  are independent  $\alpha$ -mixing fields, then  $\{F_i\}$  is an  $\alpha$ -mixing field.*

The proof follows directly from Lemma 3, as  $\alpha$ -mixing is maintained over measurable transformations and over combinations of independent  $\alpha$ -mixing random sequences. We must make the stronger assumption that  $A_i$  and  $U_i$  are independent, but given  $\alpha$ -mixing of these sequences independence establishes that  $\{F_i\}$  will also be  $\alpha$ -mixing.<sup>27</sup>

We can then show that the population sequence  $\{L_i\}$  will be  $\alpha$ -mixing as well, given an additional assumption that the market access terms  $M_i$  are also  $\alpha$ -mixing. This will ensure that the full probability space of the population distribution will be realized for large  $N$ .

**Theorem 2:** *If  $\{F_i\}$  and  $\{M_i\}$  are independent  $\alpha$ -mixing fields, then the population field  $\{L_i\}$  is  $\alpha$ -mixing.*

The proof also follows directly from Lemma 3. The  $\alpha$ -mixing of the population within the model is consistent with real-world population distributions, as large population cen-

---

<sup>25</sup>If geographic attributes were independent sequences the  $\alpha$ -mixing of  $\{A_i\}$  and  $\{U_i\}$  would follow directly from Theorem 5.2 of Bradley (2005) and  $\alpha$ -mixing of attributes with respect to distance. However, as many attributes are likely not independent, we must assume  $\alpha$ -mixing of the fundamentals with respect to distance

<sup>26</sup>We find that the correlation of the constructed “naive” fundamentals across space declines with increasing distance, as shown in Supplemental Appendix C.6, consistent with the assumption of  $\alpha$ -mixing.

<sup>27</sup>This assumption is necessary for the application of Theorem 5.2 of Bradley (2005) in the proof of Proposition 4, but we will relax this assumption in our simulations and show that it does not appear necessary for the result. Allen and Arkolakis (2014) find a low, but non-zero, correlation of 0.12 between  $A_i$  and  $U_i$  and our recovered fundamentals (discussed in the following section) have a similar correlation of 0.18.

ters tend to be surrounded by other populous areas rather than sparsely populated regions.<sup>28</sup> The  $\alpha$ -mixing of the population also implies that the very largest cities will not cluster together despite the correlations in population, because the population of different locations will approach independence as the distance between them increases.

---

<sup>28</sup>There is a literature on urban shadows which suggests that new cities tend not to form immediately next to existing cities, and which appears to be in tension with the correlation of the population distribution across space. One example of this literature is Bosker and Buringh (2017), which documents a “shadow” surrounding cities in Europe from 800-1800. This shadow is ascribed to forces beyond our model, such as the risk of armed conflict between cities, and results within Bosker and Buringh (2017) still demonstrate a high degree of spatial correlation in the population distribution (see, for example, their Figure 4). Related work on urban *growth* shadows, as in Cuberes et al. (2021) find that the growth of peripheral regions near large urban centers is influenced by the central city, with locations near urban centers tending to grow faster over the past century, which is also consistent with spatial correlation in populations.

## A.4 Population as a random variable

The system of equations describing the population distribution, given for a particular location  $i$  in Equation 17 can be expressed in matrix form as:

$$\theta \mathbf{h} = \mathbf{J}[\mathbf{h}]^{\frac{\gamma_2}{\gamma_1}} \quad (\text{A.7})$$

where  $\theta = \bar{W}^{\sigma-1}$ , each element of the vector  $\mathbf{h}$  is given by  $h_i = L_i^{\tilde{\sigma}\gamma_1}$ , and  $[\mathbf{h}]^{\frac{\gamma_2}{\gamma_1}}$  indicates raising each element of the vector  $\mathbf{h}$  to the power  $\frac{\gamma_2}{\gamma_1}$ . The matrix  $\mathbf{J}$ , where elements  $j_{i,n} = A_i^{\tilde{\sigma}(\sigma-1)} U_i^{\tilde{\sigma}\sigma} \tau_{i,n}^{1-\sigma} A_n^{\tilde{\sigma}\sigma} U_n^{\tilde{\sigma}(\sigma-1)}$ , is given by

$$J = \begin{bmatrix} j_{1,1} & j_{1,2} & \dots & j_{1,N} \\ j_{2,1} & j_{2,2} & \dots & j_{2,N} \\ \dots & \dots & \dots & \dots \\ j_{N,1} & j_{N,2} & \dots & j_{N,N} \end{bmatrix}$$

where  $\mathbf{J}$  is an  $\bar{N} \times \bar{N}$  random matrix, with its elements consisting of the realizations for fundamentals and trade costs for all locations. The vector  $\mathbf{h}$ , which consists of transformations of the population vector, is the eigenvector corresponding to the leading eigenvalue of this random matrix as shown in the online appendix to Allen and Arkolakis (2014). The eigenvectors of random matrices are themselves random vectors, which motivates our treatment of each  $L_i$  as a random variable.<sup>29</sup>

Note that each sequence  $\{s_{n,i}\}$  for a given  $i$  can be written as the vector  $\mathbf{s}_i$  resulting from the following matrix multiplication:

$$\mathbf{s}_i = \theta \mathbf{k}_i \mathbf{J}^{-1} \mathbf{h} \quad (\text{A.8})$$

where  $\mathbf{k}_i$  is a vector of elements  $k_{n,i} = \tau_{i,n}^{1-\sigma} A_n^{\tilde{\sigma}\sigma} U_n^{\tilde{\sigma}(1-\sigma)}$ .

The random vector  $\mathbf{h}$  is not the eigenvector of the random matrix  $\mathbf{K}$ . The vector  $\mathbf{s}_i$  results from the multiplication of a random vector and a random matrix, motivating the treatment of elements  $s_{n,i}$  as random variables.

---

<sup>29</sup>For a review of random matrices, see Anderson et al. (2010) and for results on eigenvectors see Ben Arous and Guionnet (2010) and O'Rourke et al. (2016).

## B Pareto vs. Lognormal, Evidence and Simulations

### B.1 More evidence on U.S. population distribution

We provide additional evidence for the lognormality of the true population by focusing on the behavior of the distribution in the tail. A potential criticism of our Figure I is that we are not using the appropriate definition of cities. We can instead consider U.S. MSAs which we do in Appendix Figure A.II. Even when considering MSAs, which prevent us from considering the distribution of the full U.S. population, we still see characteristics typical of a lognormal population distribution. There is a pronounced tendency for the right tail to fall below the trendline. Relative to expectations under the Pareto interpretation of the population distribution, this deviation amounts to a cumulative absence of 76 million people from the top 250 MSAs. The deviation would be expected under the lognormal interpretation, as shown by the size-varying scale parameter-like term discussed in Section 2.

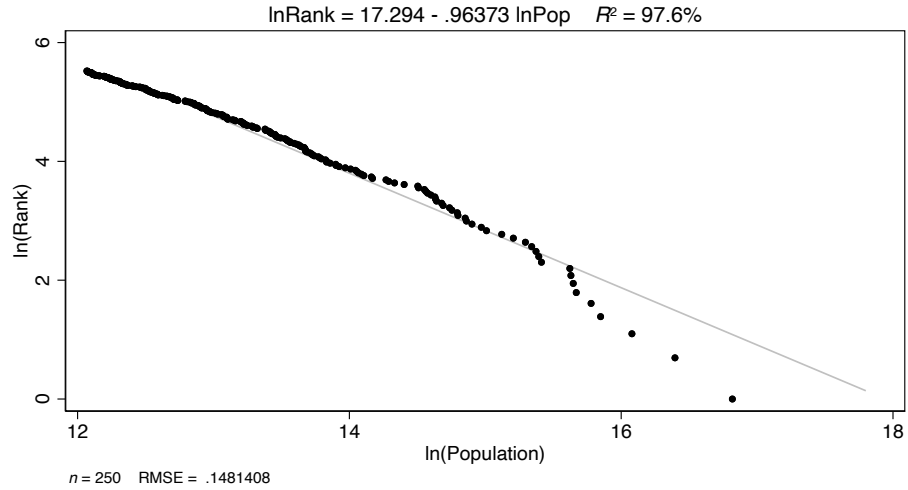
As discussed in Eeckhout (2004), one characteristic of the lognormal as compared to the Pareto is the sensitivity of the estimated coefficient to the truncation point. This can be seen in Figure A.III, where selecting alternative truncation points changes the estimated power law coefficient. The left column consists of three plots where we estimate the power law coefficient on three different subsets of the U.S. city distribution. Panel A presents the same plot as main text Figure A.II. When including more cities (Panel C) the coefficient rises, and when including fewer cities (Panel E) the coefficient falls. This is in line with the expected behavior of the scale-varying “shape parameter”-like term of the lognormal distribution in Equation 3. The  $R^2$  of all of these regressions remains similarly high. The changes in the estimated coefficient are in line with expectations if the true underlying distribution were lognormal and demonstrate that, while the -1 exponent can be found for a particular truncation point (as in Figure A.II), it does not appear to be a meaningful feature of the distribution.

In the right column of Figure A.III, we consider deviations in the far tail by excluding the top quarter of cities within each subset of the city distribution. In all cases, nearly all top quarter cities fall below the trendline predicted based on the rest of the distribution.<sup>30</sup> The magnitude of the systematic divergence is very large, which is obscured on the log scale. The deviations are larger when estimated on the subset of cities below the top quarter as in Panels B, D, and F. If the Pareto were the true distribution, panel B indicates a cumulative absence (in expectation) of 412 million people while panel D indicates a cumulative 494

---

<sup>30</sup>Of top-quarter MSAs, 62 of 62 MSAs in Panel B, 93 of 96 MSAs in panel D, and 27 of 27 MSAs in panel F are below the respective trendlines in Figure A.III

**Figure A.II: US MSAs, top 250**



*Notes:* Figure shows a log-rank, log-population plot for US Metropolitan Statistical Areas (MSAs) based on 2020 Census data. The slope is near -1, the characteristic “Zipf’s law” value often used to provide evidence of a particular Pareto interpretation of the city size distribution. Note that there is a pronounced deviation beneath the trendline in the far right tail, which is more consistent with the lognormal interpretation. Figure A.III shows that this value is very sensitive to the selected truncation point and varies depending on the subset of the data included, consistent with a lognormal interpretation of the population distribution.

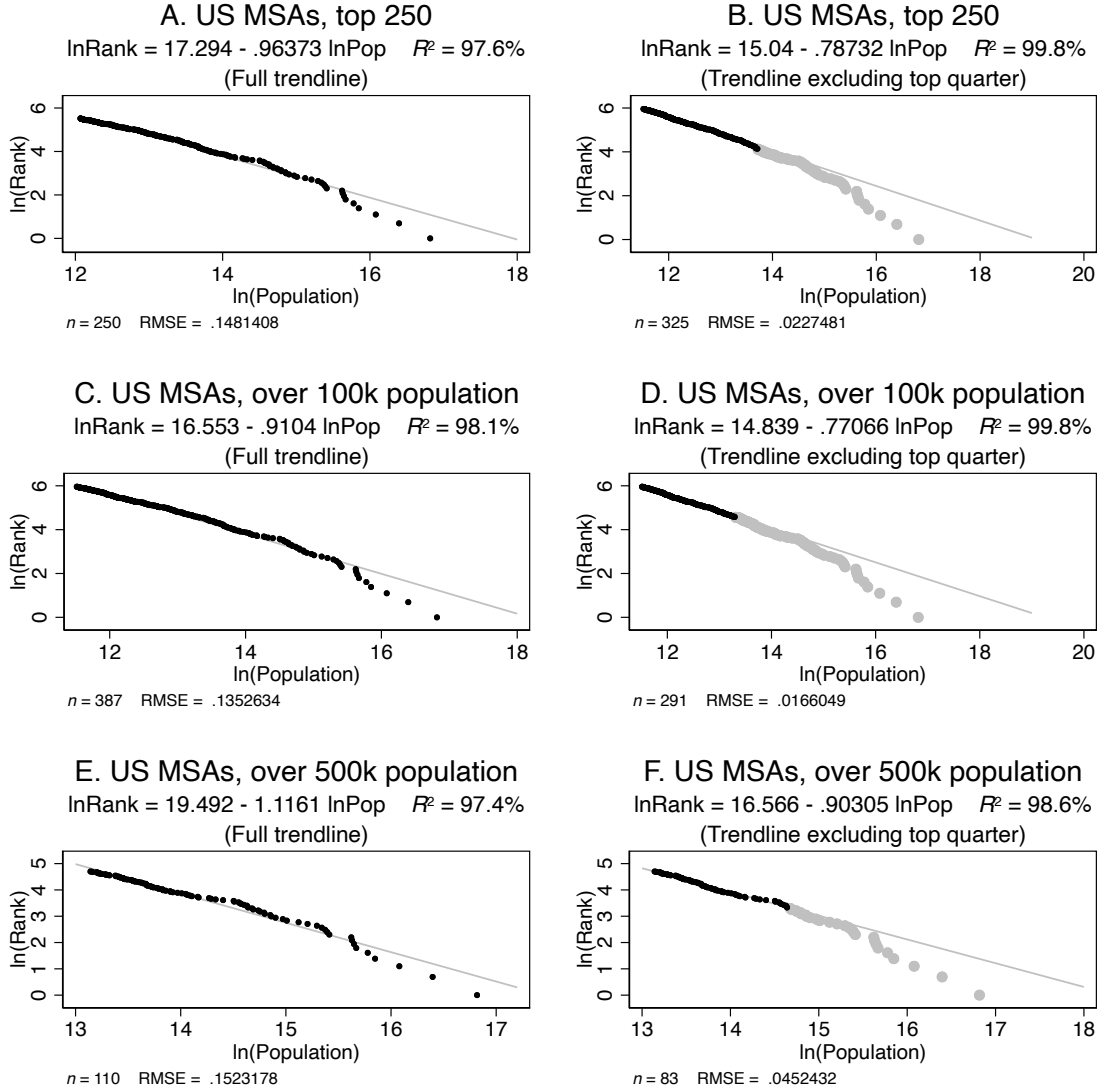
million people missing from the sets of cities considered, both substantially more than the entire U.S. population, while panel F indicates an absence of 169 million people, roughly half the U.S. population.<sup>31</sup>

This scale variance in the data offers evidence for the lognormal interpretation of the population distribution. When the true population is lognormal, large economies or regions (those containing many cities) should systematically contain smaller large cities than predicted by the estimated power law.

---

<sup>31</sup>Repeating this exercise with other large countries (India, China, and Brazil) using standardized city definitions from Dingel et al. (2021) indicates similarly large divergences in the tail, all in the expected direction (cumulative absences of 135 million, 53 million, and 8 million respectively).

**Figure A.III: Truncation Points and Power Law Coefficients**



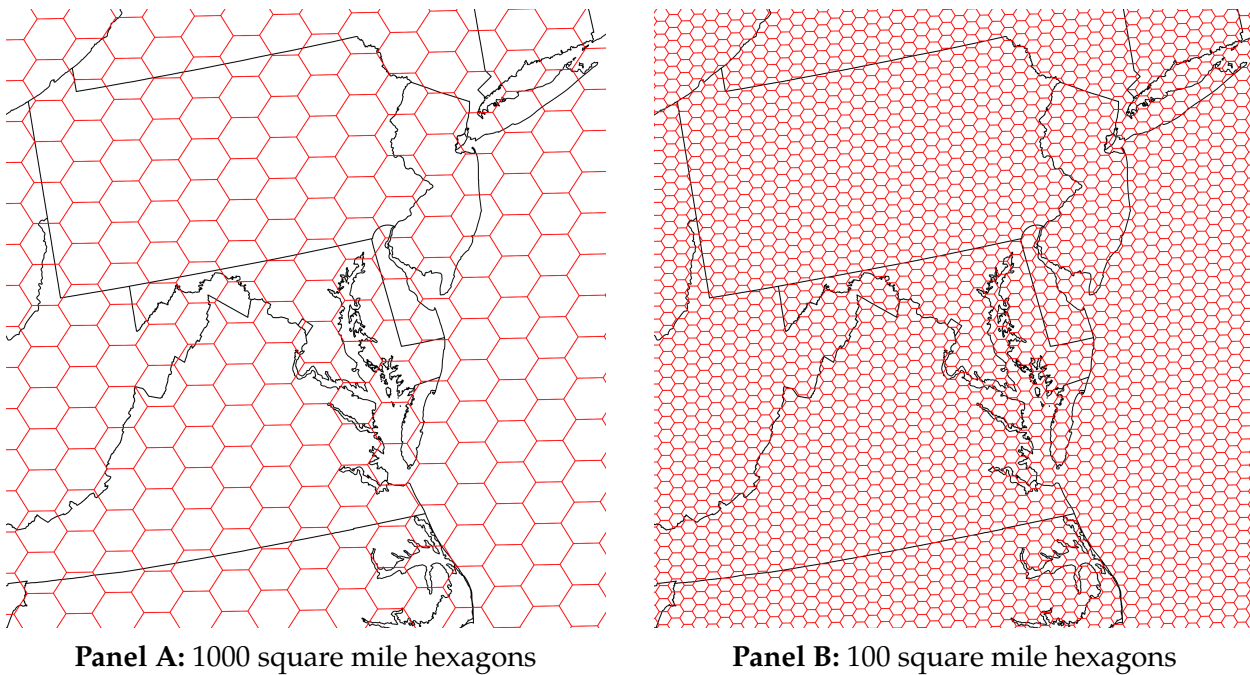
*Notes:* The panels (A—identical to Figure A.II)—and B) include the top 250 US MSAs. The middle panels (C and D) show the 388 U.S. MSAs with a population over 100k in 2020. The bottom panels (E and F) show the 110 MSAs with a population over 500k in 2020. The left column displays the trendline for the full sample the right column displays the trendline excluding the top 25% of MSAs (in grey) in each panel. Altering the truncation point substantially influences the estimated coefficient, as can be seen by contrasting the panels in the right column. Further, nearly all top quartile MSAs fall below the trendline. Excluding top quartile MSAs from the regression also substantially alters the trendline, as can be seen by contrasting the left and right columns. Both of these tendencies (changes in the regression coefficient based on truncation/excluding subsets of the data) are consistent with the U.S. city size distribution being a subset of a full lognormal distribution rather than Pareto.

## B.2 Alternative geographies: Equal area hexagons

We divide the U.S. into equal area hexagons of 1000 square miles. We keep only those hexagons that are more than 25% land, which results in 3,083 hexagons with positive population in the contiguous U.S. as the contiguous U.S. measures 2.96 million square miles. The population is constructed by aggregating the populations of 2020 U.S. census blocks based on the hexagon that each block centroid falls within. A map of the hexagons can be seen in Figure A.IV

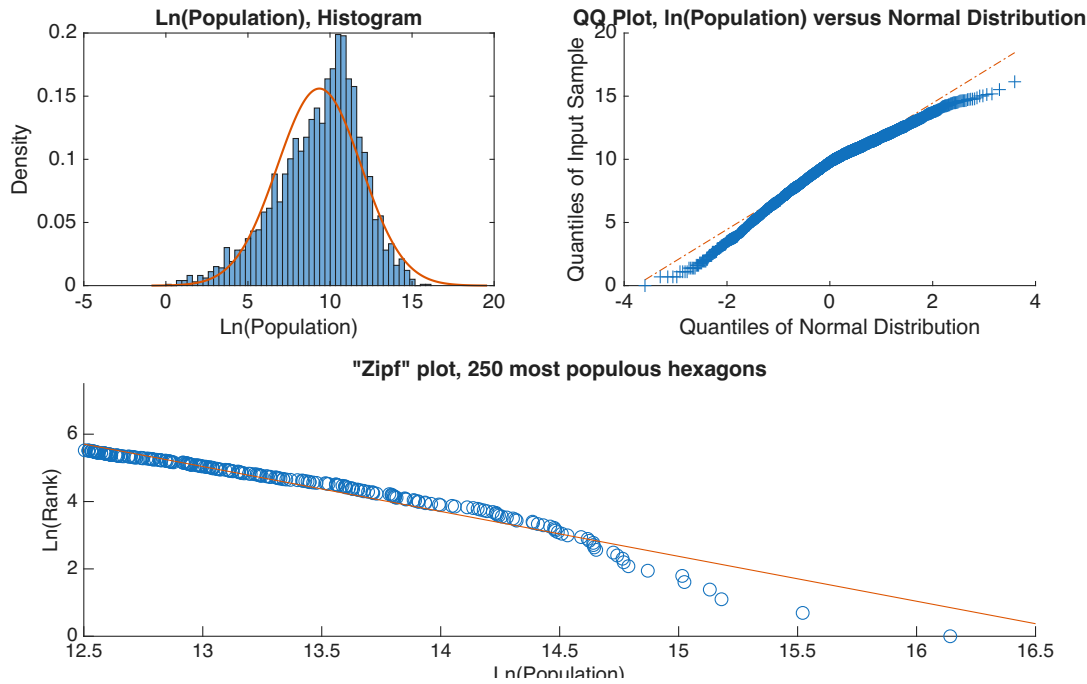
The distribution of population within both hexagons is strikingly lognormal, albeit slightly left-skewed, as can be seen in Figures A.VI and A.V. The skew may reflect the discreteness of real-world population distributions, which results in “bunching” among the lower values for the population. This bunching is more pronounced for the smaller 100 square mile hexagons, where many hexagons have only a single resident as can be seen by the flat region of the QQ plot. Beyond the modal value of each distribution, which is around 8000 people per hexagon for the 100 square mile hexagons and around 20,000 people per hexagon for the 1000 square mile hexagons, the distribution appears substantially lognormal. The right tail of the distribution appears to follow a power law as expected given the lognormal full population distribution. That this arbitrary division of the U.S. population generates a lognormal population suggests that the lognormal population distribution is some fundamental feature of human geography, not the definition of the geographic division used.

**Figure A.IV: Equal Area Hexagons**



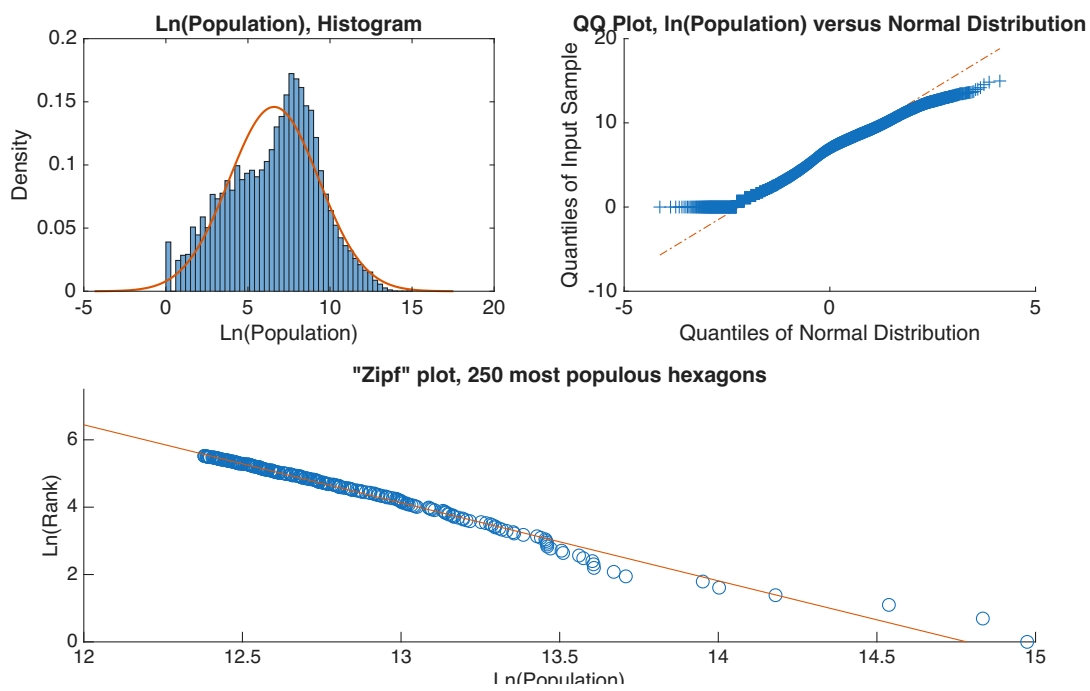
*Notes:* An example of the equal area hexagons. The map is centered on Washington, DC

**Figure A.V: 1000sq Mile Hexagons: Lognormal Populations, Power Law-like Tail**



*Notes:* The populations within 1000 square mile hexagons ( $N = 3,083$ ) appear to follow a lognormal distribution. The right tail of this distribution ( $N=250$ ) appears to follow a power law.

**Figure A.VI:** 100sq Mile Hexagons: Lognormal Populations, Power Law-like Tail



*Notes:* The populations within 100 square mile hexagons ( $N = 27,872$ ) appear to follow a lognormal distribution. The right tail of this distribution ( $N=250$ ) appears to follow a power law.

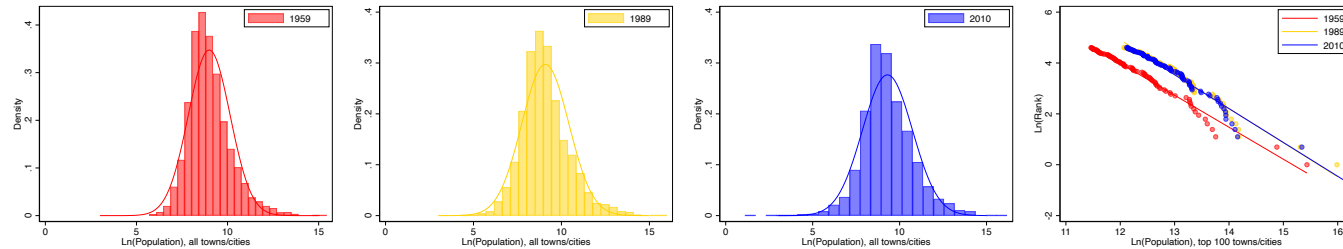
### B.3 Other contexts: Population distributions of post-Soviet states

We only observe complete and consistent geographic coverage of the population distribution in a handful of contexts. Several such contexts are the post-Soviet states. The Soviet Union conducted regular population censuses that enumerated the population of all settlements of any size, and many post-Soviet states continued conducting these surveys after the collapse of the Soviet Union. We take data on Soviet populations compiled by Tim Bespyatov on <http://pop-stat.mashke.org/>. The collected data provides complete populations down to the town level for three of the four most populous Soviet Republics in 1989. For Russia (the most populous), Ukraine (second), and Kazakhstan (fourth), in Figure B.3 we provide plots of the population in 1959, 1989, and the most recent year with complete population data in the post-Soviet period. Data is not available for Uzbekistan, the third most populous Soviet Republic as of 1989.

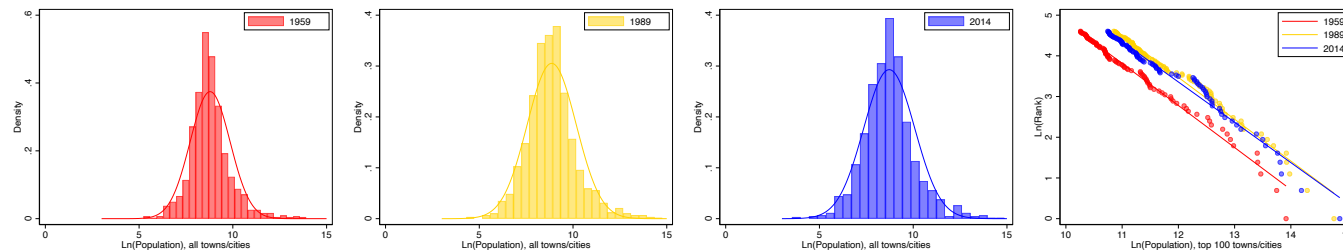
The first three columns of Figure B.3 shows that the full population distribution for each of these polities appeared to follow a lognormal distribution in all years. The fit is best for the much larger nations of Russia and Ukraine, but the lognormality of the full population distribution is still evident for Kazakhstan. In the fourth and final column we provide the log-rank, log-population plot for the three years in the three polities. Each plot shows evidence of a power law-like population distribution.

**Figure A.VII: Lognormal Populations with Power Law-like tails, Post-Soviet States**

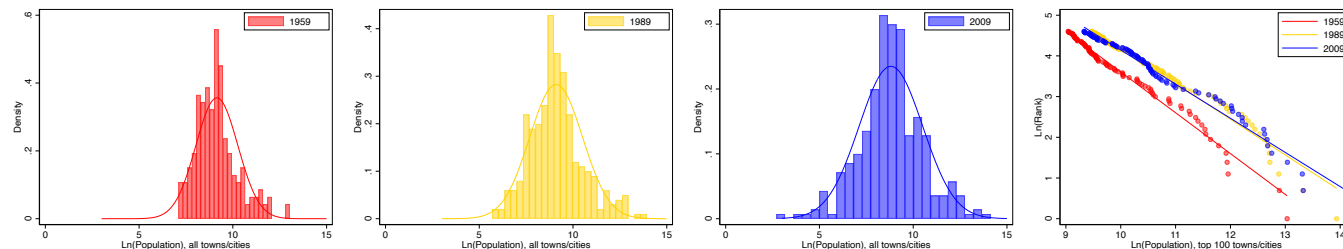
Panel A: Russia



Panel B: Ukraine



Panel C: Kazakhstan



20

Notes: Panel A plots data for Russia, Panel B for Ukraine, and Panel C for Kazakhstan. The first three columns of the three panels show the histogram of the log population distributions in 1959, 1989, and the most recent year with full population coverage. The last column shows the top 250 locations in each country in each of the plotted years. All of the histograms of fit the overlaid normal distributions well, and all of the log-rank log-population plots closely the trend lines of the associated Zipf's regression.

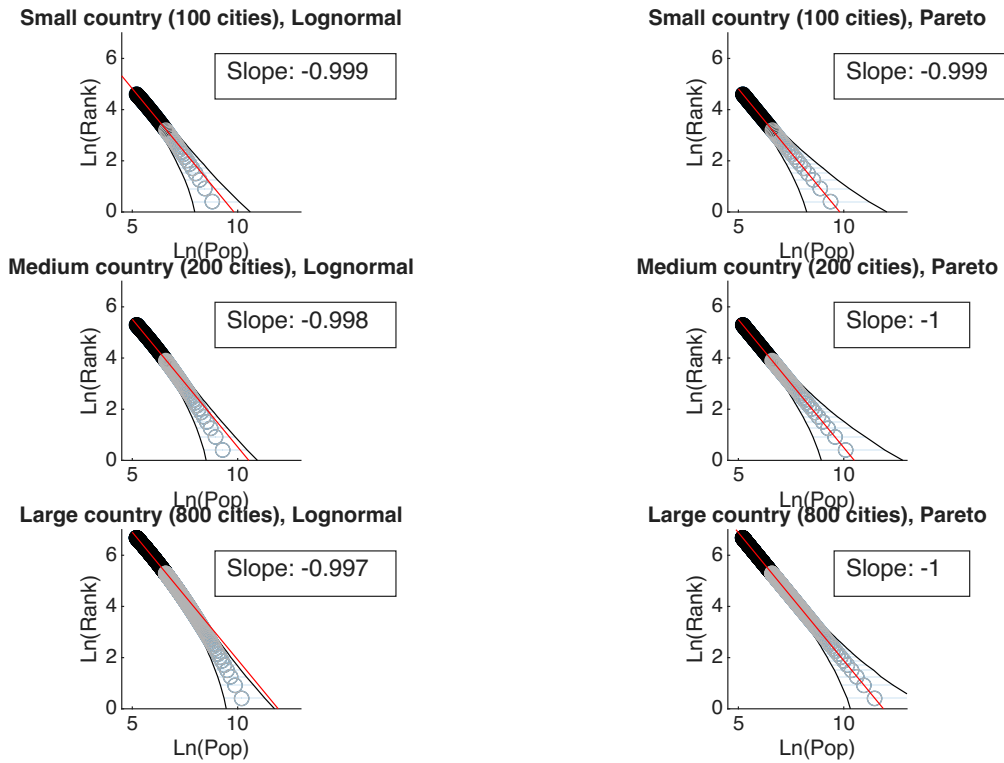
## B.4 Tail behavior of Pareto vs. Lognormal: Simulated evidence

We provide additional demonstrations of the differing scale variance of the two distributions via simulation in Figure A.VIII. We calibrate a lognormal distribution to match a Pareto distribution with shape parameter  $\alpha_P = 1$  in the tail.<sup>32</sup> The plots show the average value over 10000 draws from each distribution at each rank of the city size distribution, with the bands reflecting the 95 percent confidence interval. We calculate the slope at several scales excluding the top 25% of cities, to demonstrate the tail divergence of the lognormal resulting from its scale-variance, in contrast to the scale-invariant Pareto. When the tail is constructed to contain 100 cities (fewer overall draws), the difference between the two plots is minimal. However, when the tail is constructed to have 800 cities, cities in the far tail of the lognormal fall well below the estimated trendline.

---

<sup>32</sup>The lognormal parameters are  $\sigma_{LN} = 2.6, \mu = 0$

**Figure A.VIII:** Comparison of Lognormal and Pareto Distributions of Simulated Cities



*Notes:* Comparison of Lognormal (left) and Pareto (right) for simulated small, medium, and large “countries.” The LN is truncated for cities 2 standard deviations above  $\mu_{LN}$ , and the Pareto has a minimum value equivalent to this truncation point with shape parameter  $\alpha_P = 1$ . The slope in each plot is calculated excluding the top 25% of cities in each country, and the bands contain 95% of the observed values at each rank over 1000 simulations. When only seeing a comparatively small number of tail observations, the lognormal distribution and Pareto distribution are largely indistinguishable. However, scale variance of the LN leads to substantial divergence in the tail. At larger scales (large countries with more large cities), if the distribution is drawn from a LN distribution the large cities tend to fall below the trendline (with trend above the 95% band) while the Pareto distribution does not diverge.

## C Attributes and Fundamentals

### C.1 Data

In this section, we list the variables we used in Section 3 for our correlation matrices and tables. The data come from the publicly available data of Henderson et al. (2018).

1. *Ruggedness*: index measure of local variation in elevation. Originally computed by Nunn and Puga (2012) with corrections made in Henderson et al. (2018).
2. *Elevation*: above sea level, meters
3. *Temperature*: average from 1960-1990 of monthly temperatures, Celsius
4. *Precipitation*: average from 1960-1990 of monthly total precipitation, mm/month
5. *Land Suitability*: propensity of an area of land to be under cultivation based on separate measures of climate and soil quality
6. *Distance to Coast*: distance to the nearest coast, km
7. *Distance to Harbor*: distance to nearest natural harbor on the coast, km (great circle)
8. *Distance to River*: distance to nearest navigable river, km
9. *Malaria*: index of the stability of malaria transmission
10. *Land Area*: grid cell area covered by land,  $\text{km}^2$
11. *Growing Days*: Length of agricultural growing period, days/year

## C.2 Summary Statistics

We provide summary statistics of the attributes from Henderson et al. (2018) in Table A.I for the contiguous U.S.

**Table A.I:** Summary Statistics for Attributes

Attribute	N	Min	Max	Median	Q1	Q3	1QR	Mean	SD
Ruggedness	13,426	-2.65	1.79	0.06	-0.69	0.71	1.40	0.00	1.00
Elevation	13,426	-3.02	1.99	-0.06	-0.71	0.92	1.63	0.00	1.00
Land Suitability	13,426	-2.77	1.13	0.14	-0.55	0.91	1.46	0.00	1.00
Dist to River	13,426	-1.38	10.75	-0.25	-0.69	0.39	1.08	0.00	1.00
Dist to Coast	13,426	-0.90	4.98	-0.32	-0.60	0.23	0.84	0.00	1.00
Temperature	13,426	-3.15	2.29	-0.08	-0.76	0.83	1.60	0.00	1.00
Precipitation	13,426	-2.53	3.46	-0.12	-0.89	0.78	1.67	0.00	1.00
Dist to Harbor	13,426	-1.16	5.38	-0.32	-0.74	0.46	1.21	0.00	1.00
Growing Days	13,426	-3.12	1.54	-0.04	-0.84	0.88	1.72	0.00	1.00
Malaria Ecology	13,426	-5.60	0.56	0.51	-0.35	0.56	0.91	0.00	1.00
Land Area	13,426	-17.66	0.59	0.16	-0.03	0.32	0.34	0.00	1.00

*Notes:* Summary statistics for ordered geographic attributes for data points in the contiguous United States. Authors' calculations based on replication files of Henderson et al. (2018)

## C.3 Correlation Calculations

### Cross-Correlations

For every attribute type  $g$ , we calculate  $\text{corr}(\mathbf{a}_i, \mathbf{a}_j)$ ,  $\forall i, j \in \mathcal{G}$ ,  $j \neq g$ , where  $\mathbf{a}_g$  is a vector for each attribute type comprised of attribute values  $a_{ig}$  for every location  $i$ . This exercise tells us how correlated each attribute is with each other attribute within locations, giving an indication of how dependent realizations of geographic attributes may be on one another.<sup>33</sup>

### Spatial Correlation

To calculate spatial correlations within attributes, we construct rings at varying distances  $d$  (in miles) from every grid cell  $i$  in the contiguous U.S.; we refer to a location  $i$  around which rings are being drawn as a *centroid*. These rings define a collection of grid points in the U.S., Canada, and Mexico at a given buffered distance  $(d-10, d+10)$  for each centroid.<sup>34</sup> We then select a random point, called  $i^*(d, g)$ , from within each ring of distance  $d$  from every centroid  $i$ , to construct our sets of points to calculate the correlations; we re-draw a random point for each attribute type  $g$  for every centroid. Mathematically, our calculation for the correlation within an attribute type  $g$  between our set of centroids and our set of points at distance  $d$  takes the form  $\text{corr}(\mathbf{a}_g, \mathbf{a}_{dg})$ ,  $\forall g \in \mathcal{G}$ ,  $\forall d$ , where  $\mathbf{a}_g$  is a vector of attribute values  $a_{ig}$  for attribute type  $g$  for all centroid locations  $i$  in our sample, and  $\mathbf{a}_{dg}$  is a vector of all attribute values  $a_{i^*(d,g)g}$ , the randomly-selected points for each centroid  $i$  at distance  $d$  for each attribute type  $g$ .

---

<sup>33</sup>We do not know the full suite of attributes that characterize a location's productivity, and in our limited panel we have some attributes which are mechanically correlated within a location (such as average temperature and growing days).

<sup>34</sup>The spatial correlation in attributes between points at distance  $d = 100$  miles should be interpreted as "the correlation between a point and a randomly-selected point 90–110 miles away". The buffer is to ensure there are eligible points at roughly the desired distance.

## C.4 Empirics of Attribute Correlations

We empirically investigate the correlation of pairs of attributes within locations and the correlation of attributes across space. We provide support for our assumption of  $\alpha$ -mixing for attributes within a place, used to apply the central limit theorem above to characterize the fundamentals, and the assumption of  $\alpha$ -mixing of attributes across space, which will be used in Section 3 to characterize the population distribution.

We use gridded geographic data from Henderson et al. (2018), which includes a wide variety of first-nature geographic attributes of which we use the eleven continuous variables.<sup>35</sup> The dataset is at the quarter-degree latitude and longitude cell level.<sup>36</sup> We focus on the roughly 47,000 cells grid cells in the U.S., Mexico, and Canada, with the over 13,000 of those grid cells contained in the contiguous U.S. serving as our main sample.

First, we calculate the correlation between attributes within a given location and show that weak dependence of attributes is a reasonable assumption, as there exist pairs of attributes which do not appear correlated within places. We calculate cross-correlations between our attributes for all grid cells in the contiguous U.S., as shown in Figure A.IXa.<sup>37</sup> Our results show that the assumption of weak dependence of attributes appears reasonable given the pattern of correlations of attributes within locations. While there appears to be some correlation between some pairs of attributes within locations, the median correlation among the least-correlated attribute pairs is very near 0.

Next, we demonstrate that while there is correlation within each attribute across space, this correlation declines to zero as distance increases. We calculate spatial correlation at various distances for grid points within the contiguous U.S., as seen in Figure A.IXb.<sup>38</sup> The spatial correlation of attributes is high over short distances but as distance increases spatial correlation falls to near zero. These results suggest spatial correlation of geographic attributes does decline with distance, supporting the assumption that the fundamentals will exhibit a similar pattern of declining correlation across space.

---

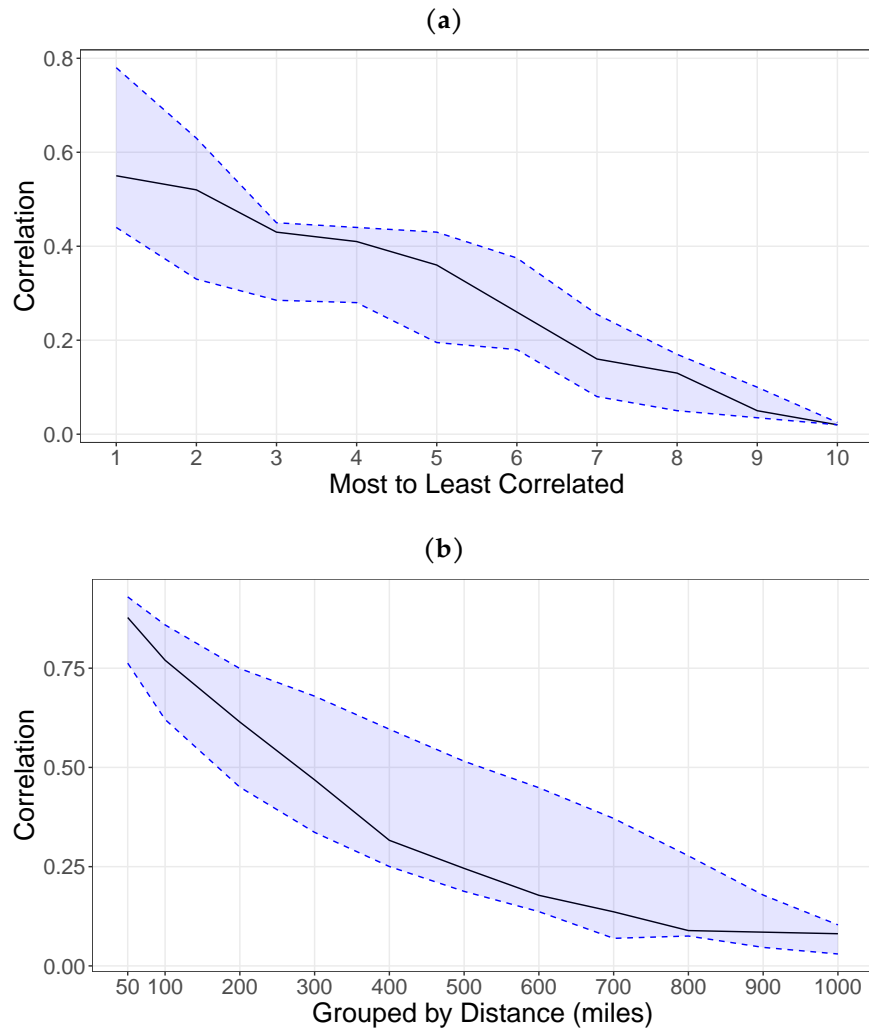
<sup>35</sup>The variables are ruggedness, elevation, land suitability for cultivation, distance to a river, distance to an ocean coast, average monthly temperature, average monthly precipitation, distance to a natural harbor, growing days per year, an index of malaria, and total land area of the grid cell. Variables in Henderson et al. (2018) that were either categorical or discrete transformations of the continuous data were excluded from our analysis.

<sup>36</sup>At the equator, a grid cell is  $\approx$ 28-by-28 km; at 48 degrees latitude,  $\approx$ 18-by-18 km.

<sup>37</sup>A description of how we calculated cross-correlation is provided in Supplemental Appendix C.3

<sup>38</sup>A description of how we calculated spatial correlation is provided in Supplemental Appendix C.3.

**Figure A.IX: Correlations Within and Across Locations**



Notes: (a) Cross-correlation and (b) spatial correlation structure of U.S. geographic attributes. The solid black line represents the median correlation; the blue dashed lines represent the 25th and 75th percentile bands. Authors' calculations based on replication files of Henderson et al. (2018)

## C.5 A “Naive” Fundamental

For every attribute in our data set which has a minimum value less than or equal to 0, we re-define the attribute using an affine transformation to put the minimum  $\approx 0.1$ . We then construct the “worst-to-best” ordering of our attribute values according to the sign on each attribute from a regression on attribute influence on economic activity as found in Henderson et al. (2018), Table 1. Attributes whose sign was positive we perform no additional transformations to. Attributes whose sign was negative we invert. We use the signs present in that table, as opposed to signs from a smaller regression of our subset of attributes on U.S. economic activity, because we believe the signs in their regression could plausibly be more robust worldwide.

After choosing our attribute value ordering, we then standardize the natural log of our attributes:

$$\hat{a}_{ig} = \frac{\ln(a_{ig}) - \text{mean}(\ln(a_g))}{\text{sd}(\ln(a_g))}$$

where  $\text{mean}(\ln(a_g))$  is the mean of that attribute across all locations and  $\text{sd}(\ln(a_g))$  is the standard deviation. This produces logged attributes which are mean 0 and standard deviation 1.

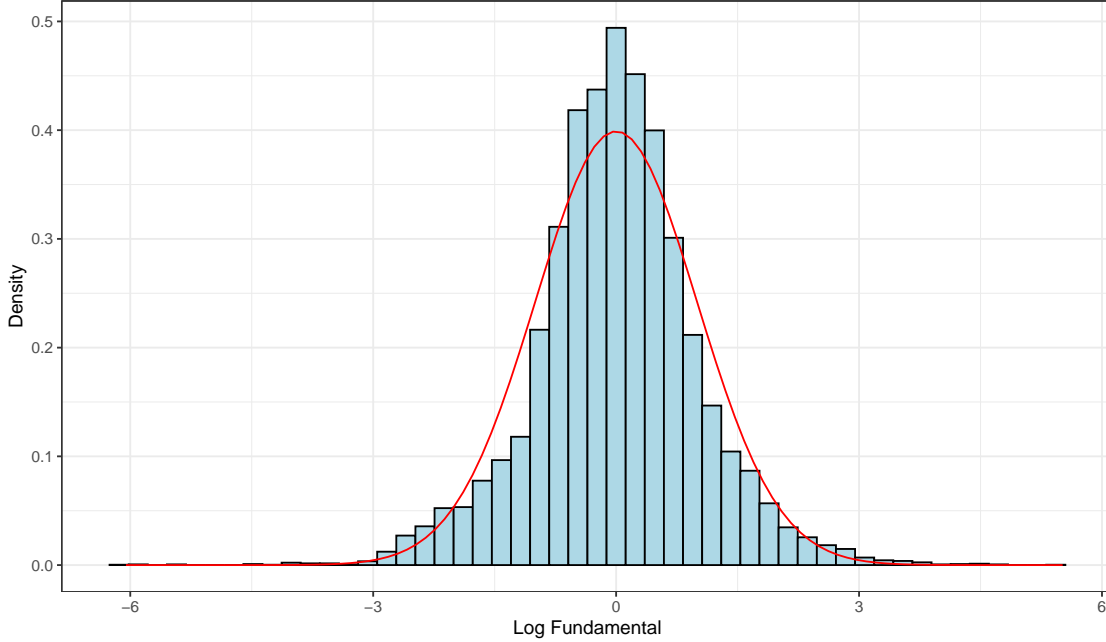
We then aggregate our attributes into a fundamental given by Equation 20:

$$\ln(A_i) = \sum_{g \in \mathcal{G}} \xi_g \hat{a}_{ig}$$

setting  $\xi_g = 1, \forall g$ .

## C.6 Results: “Naive” Fundamental and Correlations

**Figure A.X:** Lognormal Distribution of “Naive” Locational Fundamentals



*Notes:* Lognormal distribution of locational fundamentals for Contiguous U.S. All eleven attributes were ordered worst to best in terms of contribution to economic activity, logged, then standardized. The fundamental is calculated as the standardized sum of the standardized, ordered log attributes. The attributes are at the grid-cell level ( $N = 13,426$ ). The mean and variance are standardized to zero and one and a standard normal curve is overlaid. Authors’ calculations based on replication files of Henderson et al. (2018)

We plot in Figure A.X the empirical PDF of the resulting distribution of productivity fundamentals, calculated according to Equation 20 with  $\xi_g = 1, \forall g$ . The log of the empirical “fundamental” here is closely fit by a normal distribution, supporting the claim that aggregating weakly dependent and spatially correlated attributes can result in lognormal fundamentals, both in theory and in the data.

Additionally, we calculate the spatial correlation of the logged fundamental over distance for the contiguous U.S. The table of correlation values, provided in Table A.II, shows declining correlation over distance, consistent with our theoretical predictions and in line with the spatial correlation declines which appear for geographic attributes (provided in the main text).

**Table A.II:** Spatial Correlation of “Naive” Fundamental for the Contiguous U.S.

Distance (mi)	Correlation
50	0.727301
100	0.586996
200	0.409837
300	0.280963
400	0.187285
500	0.147945
600	0.117534
700	0.010313
800	-0.055472
900	-0.067386
1000	-0.067446

*Notes:* The table indicates declining correlation towards 0 over distance of our logged fundamental, in line with theoretical predictions. Given randomness in the correlation calculation process, spurious and small deviations from 0 at large distances are possible. Authors’ calculations based on replication files of Henderson et al. (2018).

## D Model Inversion

### D.1 Main inversion: U.S. counties

This appendix discusses our empirical portion, which recovers fundamentals using data on wages and populations for US counties and estimated trade costs. Our model inversion largely follows Allen and Arkolakis (2014), with slight modifications to suit the new data we use and our interpretation of the model primitives.

We draw on three data sources for county attributes. We use the 2020 decennial census for information on the total population in the county each county's demographic make-up. We use the American Community Survey (ACS) from 2020 for average county incomes. We use the Facebook Social Connectedness Index (SCI) for a measure of the degree of social connection between pairs of counties (Bailey et al. 2018). The SCI provides a normalized score reflecting the probability that any a Facebook user in county A and a Facebook user in county B would be "friends" on the social network.

We combine these county data with data on trade costs from the 2017 Commodity Flow Survey (CFS) in order to estimate county-county trade costs. We follow Allen and Arkolakis (2014) in using a discrete choice estimation of the relative trade costs for various modes based on mode-specific shares. The three modes we consider are road, rail, and water. We exclude air, which was included in the original Allen and Arkolakis (2014) inversion, as very few CFS pairs record trade via this mode and the distances recorded in the 2017 CFS make it clear that most of this trade is not direct, such that it is difficult to calculate the distances on a travel map without knowledge of the hub-and-spoke system of air trade in the US.

We use three travel maps for our three modes. We draw on the TIGER/Line primary roads map for 2019, from which we extract the Interstate Highway System. We then complement this with the TIGER/Line primary-secondary road network for a complete road network. We use the TIGER/Line railway map for 2019 for rails. We use a map of water shipping routes from the US DOT for water routes. We convert each of these maps into an equal distance raster with cells 5km across, and assign each cell in the raster a travel speed. For roads, we assign the highest speed (70 mph) to interstate highways, a medium speed to other roads (35 mph), a low speed to travel off-road (10 mph), and a negligible speed to travel off-land (0.1 mph). For trains we assign a high speed (50 mph) to travel on rail and the same land and off land speeds as for road travel. For water, we assign a high speed (20 mph) to travel on a designated water shipping route, a lower speed to travel on water outside a shipping route (10mph), and a low speed to travel on land (1 mph). We use the Matlab image processing tool to obtain the distance between all counties in the US

by each of these three modes.

To construct the distance between CFS regions, we follow Head and Mayer (2009) and construct the CFS distances as a CES combination of the population-weighted distances between all of the constituent counties of each CFS region. This provides a better sense of both the distances between two different CFS regions as well as an internal distance for each CFS region. Given our normalization of distances, we do not follow Head and Mayer (2009) in assigning each county a distance to itself based on its land area but simply set this to the shortest such distance by each mode observed in the data.

We estimate the relative trade costs as in Allen and Arkolakis (2014) by finding the variable (for road, rail, and water) and fixed (for rail and water) costs that best rationalize the observed mode shares based on a discrete-choice model of trade. There is a mass of identical traders for each origin  $i \in \mathcal{N}$ , and they choose a mode of transportation that minimizes trade costs of shipping some unit amount of the consumption good from  $i$  to any destination  $n \in \mathcal{N}$ . For  $m \in M = \{\text{Road}, \text{Rail}, \text{Water}\}$ , we assume that the cost of using each mode for trader  $t$  takes the form  $\exp(v_m d_{i,n}^m + f_m + \nu_{mt})$ , where  $\nu_{mt}$  is a mode-specific idiosyncratic cost that is distributed i.i.d. Gumbel across traders and modes with a shape parameter  $\theta$ . This means that we can express the share of trade shipped by each mode as:

$$\pi_m(i, n) = \frac{\exp(-a_m d_{i,n}^m - b_m)}{\sum_{l \in M} \exp(-a_l d_{i,n}^l - b_l)} \quad (\text{A.9})$$

Where  $a_m = v_m \theta$  and  $b_m = f_m \theta$ . We recover estimates of  $a_m$  and  $b_m$  in the first stage of our estimating procedure by finding the parameter estimates that best match the observed mode shares in the data.

The recovered first-stage trade costs must be normalized by an estimate of  $\theta$ , which we recover in the next step of our estimating procedure. Within the discrete choice framework, the average geographic trade cost will be given by:

$$\tau_{i,n}^g = \frac{1}{\theta} \Gamma\left(\frac{1}{\theta}\right) \left( \sum_M \exp(-a_m d_{i,n}^m - b_m) \right)^{-\frac{1}{\theta}} \quad (\text{A.10})$$

Using our estimated a PPML regression to recover the parameter  $\theta$  that allows us to calculate average geographic trade costs. Taking logs of equation 11, and assuming that trade costs  $\tau_{i,n} = \tau_{i,n}^g \cdot \tau_{i,n}^{ng}$ , where  $\tau_{i,n}^{ng}$  are non-geographic trade costs captured by a vector of bilateral observables  $C_{i,n}$ , we estimate the following gravity equation:

$$\ln X_{i,n} = \frac{\sigma - 1}{\theta} \ln \sum_M \left( \exp(-\hat{a}_m d_{i,n}^m - \hat{b}_m) \right) + (1 - \sigma) \beta' \ln \mathbf{X}_{i,j} + \delta_i + \delta_n + C + \epsilon_{i,n} \quad (\text{A.11})$$

By fixing the elasticity  $\sigma = 5$  we can recover an estimate for  $\theta$  from the coefficient on the first term and an estimate for non-geographic trade costs from  $\beta$ . The “non-geographic” trade costs we include in  $\mathbf{X}_{i,n}$  are 1) an indicator variable reflecting if the two CFS regions are in the same state, 2) the difference in log incomes between the CFS regions, 3) the strength of social connectedness between the two regions, constructed as an indicator if the two CFS regions are both in each other’s the top quartile of connectiveness 3) several controls to reflect racial differences (the difference in a normalized racial similarity index, along with the difference in share black, white, and Asian), and 4) several control to reflect differences in industrial composition (the difference in a normalized industrial similarity index, along with the difference in share agriculture and share manufacturing).

We estimate the coefficients using a PPML regression, to deal with frequent 0s in the trade data between CFS regions. We then obtain the estimated coefficient values by setting  $\sigma = 5$  to recover  $\hat{\theta}$  and the vector  $\hat{\beta}$ . We report bootstrap standard errors (1000 replications of the estimating procedure) for all coefficients. Our results are reported in Table A.III.

The values we find are generally half the size of those in the Allen and Arkolakis (2014) inversion, reflecting the different value of  $\sigma$  we adopt (their inversion used  $\sigma = 9$ ). We use these trade costs and the distances between all counties by each mode to construct a matrix of county-county trade costs. As county-county differences are often much more extreme than CFS-CFS differences, as CFS regions are much larger and differ less along the dimensions that determine our non-geographic trade costs, we winsorize the non-geographic trade costs for counties at one standard deviation above the mean of the non-geographic trade costs for CFS regions. Given these trade costs, we invert the model and recover the exogenous  $A_i$  and  $U_i$  for each location, using  $\alpha = 0.03$  and  $\beta = -\frac{1}{3}$  for all US counties. The distributions of the resulting fundamentals, own-fundamentals  $F_i$  term, and market access  $M_i$  term are given in the main text in Figure II.

**Table A.III:** Estimated mode-specific relative costs

	Road	Rail	Water
Variable cost	1.2821*** (0.0554)	0.0381* (0.0231)	0.0032 (0.0254)
Fixed cost		1.1893*** (0.0569)	1.4863*** (0.0714)
Estimated shape parameter ( $\hat{\theta}$ )		6.7281*** (0.3359)	
Same state		-0.3069*** (0.0169)	
Difference in $\ln(\text{avg. income})$ , abs. value		0.2332*** (0.0557)	
Highly connected (SCI)		-0.1397*** (0.0165)	
Racial difference index		1.2575*** (0.2198)	
Difference, share black		-0.1916 (0.2506)	
Difference, share white		0.5116*** (0.1308)	
Difference, share asian		0.0620 (0.3251)	
Industry difference index		-1.8895*** (0.1108)	
Difference, share agriculture		6.2598** (2.4475)	
Difference, share manufacturing		-1.8476*** (0.2627)	
Pseudo R2		.899	
Observations (positive mode-specific flows)	11297	1185	149
Observations (positive flows)		11453	
Observations		16641	

*Notes:* The table shows the parameter values resulting from our two-stage estimation of trade costs. The estimation consists of a first-stage discrete choice estimate, with a PPML regression of trade flows between CFS regions on the resulting unscaled trade costs in the second stage. Bootstrap standard errors are reported in parentheses.

## D.2 Secondary inversion: Equal area hexagons

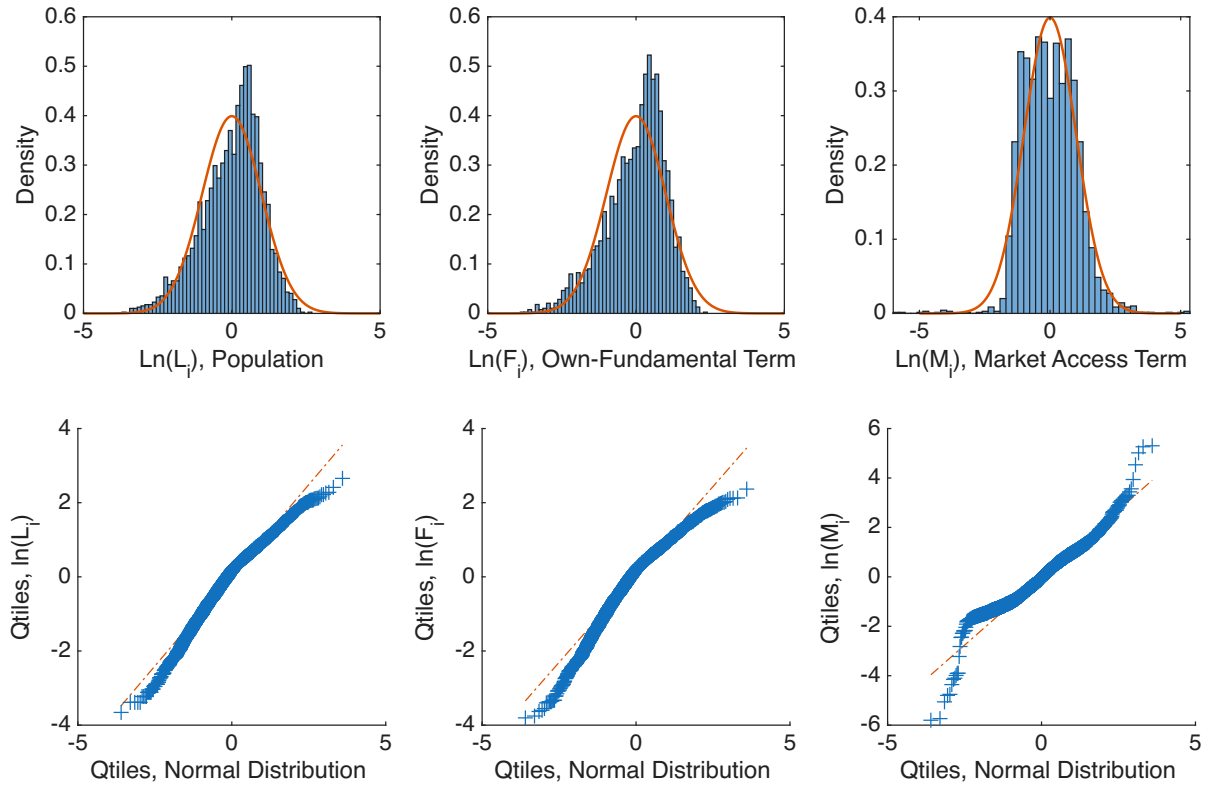
We perform the inversion on an alternative geographic division of the U.S. population. Counties provided a convenient unit because they cover the full U.S. population and a large amount of data is reported at the county level. However, the model is not explicit about the level of geography at which the geography should be done beyond it being the level at which the local agglomeration and congestion spillovers occur.

We use the division of the U.S. population into equal area hexagons as shown in Figure A.IV. This minimizes the variation in land area across the hexagons, such that density and population are more strongly correlated than in the county-level data. This is attractive, as the agglomeration and congestion costs may depend on density rather than just the overall population of a large region.

We use the same travel maps as for the primary inversion on U.S. counties, calculating the travel times between the centroids of the hexagons. We construct the population of the hexagons by using data on U.S. census blocks from 2020, the smallest level of geographic aggregation with population data. We match census blocks to hexagons using the latitude and longitude of the census block. We then construct hexagon-level measures of the controls we use in our primary inversion using the block-level populations to provide weights. We construct income and race measures from the ZCTA-level ACS data, the lowest level of spatial aggregation at which this information is available. We construct the industrial composition of the hexagons from the county-level CBP data.

The results of the inversion can be see in Figure A.XI. Fundamentals recovered from this inversion look lognormal, as does market access. Deviations from the lognormal plot in the tails are more pronounced with this arbitrary geography than for the county-level inversion, but the fit is still quite good for most of the distribution.

**Figure A.XI:** Hexagons: Populations, Recovered Fundamentals, and Resulting Market Access



*Notes:* The figure shows the distribution of population across US counties along with the distributions of the recovered own-fundamental terms  $F_i$  and the market access terms  $M_i$ . All of the distributions have been normalized for comparison against a standard normal distribution. The distribution of the recovered terms appear lognormal, as predicted by the theory.

## E Simulation Details

This section gives more details on the simulation. We first discuss the main simulation and then discuss the version of the simulation where we vary parameter values.

### E.1 Main simulation

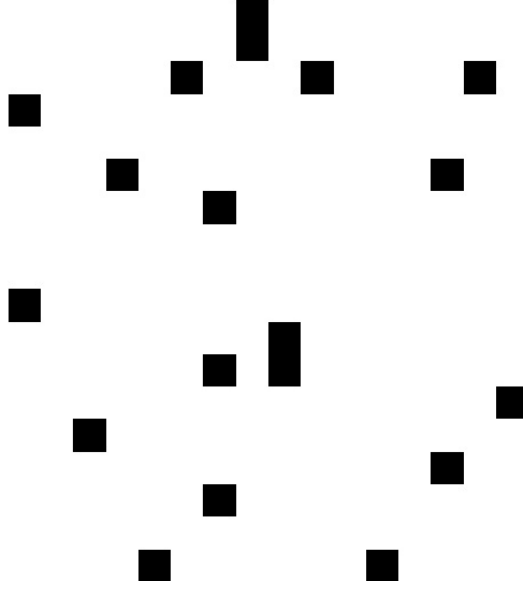
In our simulations, we take exogenous parameters  $\alpha$ ,  $\beta$ , and  $\sigma$  from the literature and parameterize the remaining values based on our model inversion. The magnitude of local productivity spillovers is given by  $\alpha = 0.03$ , in line with the estimates in Combes et al. (2008) and those surveyed in Rosenthal and Strange (2004) and Combes and Gobillon (2015). To parameterize  $\beta$ , we use an isomorphism in the model which we use to parameterize congestion costs. As discussed in Allen and Arkolakis (2014), the model is isomorphic to one with a fixed quantity of housing where spending on housing is  $\delta$  and  $\beta = -\frac{\delta}{1-\delta}$ . Congestion costs are parameterized to match a level of spending on housing of 25% of income, which gives a congestion parameter of  $\beta = -\frac{1}{3}$ , consistent with the estimates in Combes et al. (2019) and Davis and Ortalo-Magné (2011). We take the value of  $\sigma = 5$ , as used in Redding and Rossi-Hansberg (2017) based on estimates from Simonovska and Waugh (2014).

We model settlements as occurring randomly over a large surface and take the Euclidean distance between all settlements. We take draws from uniform distributions with parameters  $[1, a]$  where  $a$  reflects the maximal horizontal and vertical dimension of our full square geography. We take draws until we have realized a set number of locations within the full geography. Figure A.XII shows the locations in the center of our geography to provide an example of the realized “dartboard.” Using a dartboard geography is convenient because it allows us to ensure trade costs respect the triangle inequality, ensures random variation in trade costs, and obviates the need to calculate least-cost paths beyond taking the Euclidean distance between points. In our main simulated results, we take a new draw of settlement locations for each simulation.

We simulate a large geography and take the central locations as the geography of interest to limit the impact of border effects on the population distribution. We uniformly distribute 500 settlements across a 100-by-100 grid. In order to ensure that trade costs are not skewed by location near the edge of the geography, we create a buffer region with a width equal to the central geography, and distribute an equal density of settlements over this buffer region. This results in us simulating the geography for a 300-by-300 grid with 4500 settlements (500 in the center, 4000 in the periphery).

The remaining parameters are drawn from our inversion exercise. We set the distance

**Figure A.XII:** Example of “Dartboard” Geography



*Notes:* The figure shows the middle settlements of our full geography to provide an example of how we induce variation in trade costs.

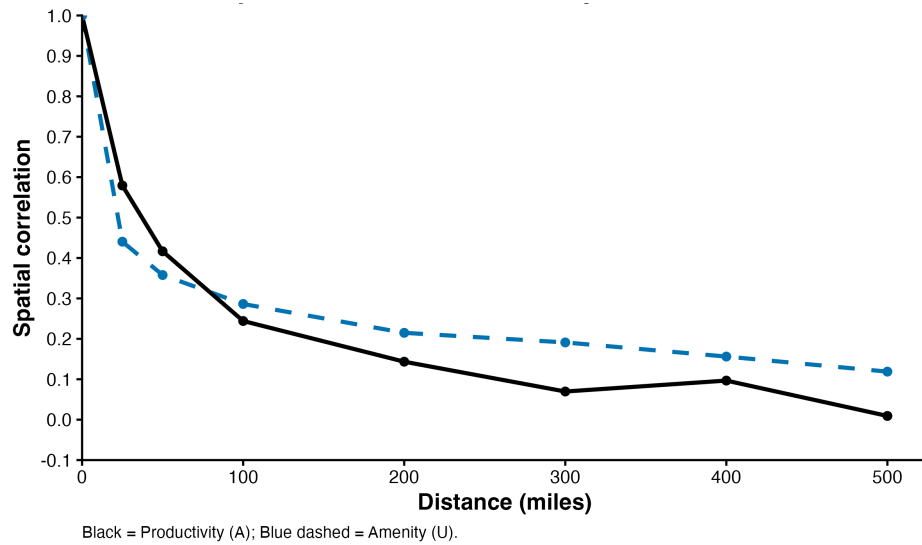
across the central 100-by-100 geography equal to 1, which allows us to use parameters estimated from the model inversion to parameterize the simulation. We parameterize the correlation of  $A_i$  and  $U_i$  within a location ( $\rho_{AU}$ ), the rate of decay in the correlation of fundamentals over space ( $\delta_{corr}$ , and the rate of increase in trade costs with distance ( $\delta_{TC}$ ) based on the model inversion. We observe  $\rho_{AU}$  directly in the inversion output. We estimate  $\delta_{corr}$  using equation A.12, after calculating the spatial correlations in fundamentals using the same procedure as in Appendix C.3. The results are shown in Table A.V, and a plot of the calculated correlations can be seen in Figure A.XIII. We estimate  $\delta_{TC}$  using equation A.13 on the CFS data after calculating the geographic trade costs as in equation A.10. The results are shown in Table A.IV.

$$\rho_{dist} = \delta_0 + \delta_{corr} dist + \epsilon_{dist} \quad (\text{A.12})$$

$$\ln(\tau^G) = \delta_0 + \delta_{TC} dist_{ij} + \epsilon_{ij} \quad (\text{A.13})$$

Fundamentals are drawn from lognormal distributions with parameters as given in Table I, based on our inversion. We induce correlation in fundamentals within a location and spatial correlation in fundamentals between locations using Choleski decompositions

**Figure A.XIII:** Spatial correlation in fundamental, various distances



*Notes:* The figure shows the estimated spatial correlation in  $A_i$  and  $U_i$  at 25, 50, 100, 200, 300, 400, and 500 miles. The spatial correlation of the fundamentals is high at short distances but declines as distance increases.

**Table A.IV:** Regression of estimated geographic trade costs on distance

	(1)
	Ln(Geographic Trade Cost)
Distance (normalized)	1.204*** (927.46)
Constant	-0.0354*** (-64.34)
$R^2$	0.981
Observations	16641

*Notes:* The figure shows the middle settlements of our full geography to provide an example of how we induce variation in trade costs.

**Table A.V:** Regression of spatial correlation in fundamentals

	(1)	(2)
	$A_i$	$U_i$
Distance (normalized)	-20.927*** (2.952)	-9.046*** (1.854)
Constant	-0.336 (0.277)	-0.649*** (0.174)
$R^2$	0.893	0.799
Observations	8	8

*Notes:* The table shows a regression on the data in Figure A.XIII.

based on our parameterizations of  $\rho_{AU}$  and  $\delta_{TC}$ .

## E.2 Additional simulations: Varying Parameter Values

In the simulations for varying parameter values, we take all combinations of  $\alpha = [0.02, 0.04, 0.06, 0.08, 0.1]$ ,  $\beta = [-0.25, -0.30, -0.35, -0.40, -0.45, -0.50]$ , and  $\delta_{TC} = [0.75, 1.00, 1.25, 1.50, 1.75]$ . For each combination, we find the population distribution for 100 draws of the exogenous geography in a grid of the same dimensions as for our main results.

We here report the full table of estimated parameter values for three values of  $\delta_{TC}$ , at 0.75, 1.25, and 1.75. When increasing  $\alpha > 0$ , the coefficient tends to increase (flatter slope). When increasing  $\beta < 0$ , the coefficient tends to increase (flatter slope). When increasing  $\delta_{TC} > 0$ , the coefficient tends to increase (flatter slope). As can be seen in Tables A.VI (showing average coefficients) change is nearly always in the anticipated direction between simulations.

To get the signs for the comparative statics reported in Table III, using the average estimated coefficient  $\hat{\theta}_i$  from each of the 150 combinations of parameters we estimate the following regression:

$$\hat{\theta}_i = \psi_1 \alpha_i + \psi_2 \beta_i + \psi_3 \delta_{TC,i} + \epsilon_i \quad (\text{A.14})$$

where the estimated coefficients  $\hat{\psi}_1$ ,  $\hat{\psi}_2$ , and  $\hat{\psi}_3$  are estimates of  $\frac{\partial \theta_1}{\partial \alpha}$ ,  $\frac{\partial \theta_1}{\partial \beta}$ , and  $\frac{\partial \theta_1}{\partial \theta}$ , respectively. The signs of these coefficients are reflected in Table III, and the full regression output is included in Table A.VII.

Notably, the estimated coefficients are consistently in the neighborhood of -1 throughout the parameter space we simulate here. Given alternative truncations of the distribution (either expanding or reducing the number of locations included, as discussed in Eeckhout (2004)) achieving a -1 slope is likely possible for most of these parameter combinations.

**Table A.VI:** Changes to Mean Power Law Coefficient through Model Parameters

**Panel A:**  $\delta_{TC} = 0.75$

	$\beta = 0.25$	$\beta = 0.30$	$\beta = 0.35$	$\beta = 0.40$	$\beta = 0.45$	$\beta = 0.50$
$\alpha = 0.02$	-1.036 (0.227)	-1.141 (0.230)	-1.278 (0.282)	-1.324 (0.279)	-1.509 (0.335)	-1.634 (0.309)
$\alpha = 0.04$	-0.986 (0.214)	-1.086 (0.203)	-1.248 (0.236)	-1.355 (0.278)	-1.517 (0.306)	-1.586 (0.298)
$\alpha = 0.06$	-0.922 (0.211)	-1.087 (0.224)	-1.181 (0.246)	-1.259 (0.247)	-1.467 (0.302)	-1.540 (0.319)
$\alpha = 0.08$	-0.905 (0.197)	-1.040 (0.200)	-1.110 (0.229)	-1.242 (0.249)	-1.381 (0.290)	-1.539 (0.318)
$\alpha = 0.10$	-0.891 (0.216)	-0.993 (0.239)	-1.051 (0.248)	-1.264 (0.262)	-1.353 (0.249)	-1.497 (0.311)

**Panel B:**  $\delta_{TC} = 1.25$

	$\beta = -0.25$	$\beta = -0.30$	$\beta = -0.35$	$\beta = -0.40$	$\beta = -0.45$	$\beta = -0.50$
$\alpha = 0.02$	-0.995 (0.215)	-1.046 (0.234)	-1.187 (0.272)	-1.307 (0.288)	-1.486 (0.337)	-1.636 (0.377)
$\alpha = 0.04$	-0.941 (0.223)	-1.035 (0.225)	-1.179 (0.248)	-1.335 (0.298)	-1.425 (0.323)	-1.521 (0.323)
$\alpha = 0.06$	-0.841 (0.185)	-1.001 (0.224)	-1.110 (0.261)	-1.302 (0.250)	-1.368 (0.298)	-1.472 (0.326)
$\alpha = 0.08$	-0.808 (0.200)	-0.940 (0.236)	-1.062 (0.236)	-1.142 (0.252)	-1.362 (0.265)	-1.464 (0.325)
$\alpha = 0.10$	-0.768 (0.162)	-0.953 (0.226)	-1.111 (0.244)	-1.192 (0.267)	-1.298 (0.267)	-1.402 (0.301)

**Panel C:**  $\delta_{TC} = 1.75$

	$\beta = -0.25$	$\beta = -0.30$	$\beta = -0.35$	$\beta = -0.40$	$\beta = -0.45$	$\beta = -0.50$
$\alpha = 0.02$	-0.934 (0.229)	-1.052 (0.240)	-1.205 (0.278)	-1.324 (0.280)	-1.501 (0.319)	-1.588 (0.368)
$\alpha = 0.04$	-0.901 (0.198)	-1.007 (0.246)	-1.146 (0.247)	-1.241 (0.279)	-1.366 (0.276)	-1.439 (0.305)
$\alpha = 0.06$	-0.816 (0.185)	-0.963 (0.233)	-1.133 (0.259)	-1.228 (0.280)	-1.382 (0.307)	-1.498 (0.316)
$\alpha = 0.08$	-0.775 (0.204)	-0.907 (0.210)	-1.023 (0.248)	-1.236 (0.272)	-1.313 (0.330)	-1.453 (0.327)
$\alpha = 0.10$	-0.730 (0.186)	-0.913 (0.194)	-1.038 (0.230)	-1.111 (0.260)	-1.275 (0.298)	-1.349 (0.283)

*Notes:* Table containing the average coefficient over 100 simulations on the exogenous geography. The standard deviation of the estimated coefficient over the 100 simulations is in parentheses.

**Table A.VII:** Regressions of MC Zipf's coefficients on parameter combinations

	Zipf's Coefficient Estimate			
	(1)	(2)	(3)	(4)
$\alpha$	2.115*** (0.635)			2.115*** (0.0843)
$\beta$		2.509*** (0.0709)		2.509*** (0.0279)
$\delta$			0.0899* (0.0522)	0.0899*** (0.00675)
Constant	-1.324*** (0.0421)	-0.256*** (0.0273)	-1.309*** (0.0677)	-0.495*** (0.0146)
Adjusted $R^2$	0.063	0.894	0.013	0.983
Observations	150	150	150	150

*Notes:* The table shows regressions corresponding to Equation A.14. The signs of the coefficients are reported in main text Table III

## Appendix References

- Allen, T. and Arkolakis, C. (2014). Trade and the Topography of the Spatial Economy. *Quarterly Journal of Economics*, 129(3):1085–1140.
- Anderson, G., Guionnet, A., and Zeitouni, O. (2010). *An Introduction to Random Matrices*. Cambridge Studies in Advanced Mathematics. Cambridge University Press.
- Ben Arous, G. and Guionnet, A. (2010). Wigner matrices, pages 433–451. Oxford University Press.
- Bradley, R. C. (1993). Equivalent mixing conditions for random fields. *The Annals of Probability*, 21(4):1921–1926.
- Bradley, R. C. (2005). Basic Properties of Strong Mixing Conditions. A Survey and Some Open Questions. *Probability Surveys*, 2(N.A.).
- Dingel, J. I., Mischio, A., and Davis, D. R. (2021). Cities, lights, and skills in developing economies. *Journal of Urban Economics*, 125:103174.
- Doukhan, P. (1994). *Mixing: Properties and Examples*. Lecture notes in statistics. 3 Island Press.
- Eeckhout, J. (2004). Gibrat's Law for (All) Cities. *American Economic Review*, pages 1429–1451.
- Giesen, K., Zimmermann, A., and Suedekum, J. (2010). The size distribution across all cities—double Pareto lognormal strikes. *Journal of Urban Economics*, 68(2):129–137.
- Henderson, J. V., Squires, T., Storeygard, A., and Weil, D. (2018). The Global Distribution of Economic Activity: Nature, History, and the Role of Trade. *The Quarterly Journal of Economics*, 133(1):357–406.
- Ioannides, Y. and Skouras, S. (2013). US city size distribution: Robustly Pareto, but only in the tail. *Journal of Urban Economics*, 73(1):18–29.
- Marlow, N. (1967). A Normal Limit Theorem for Power Sums of Independent Random Variables. *Bell System Technical Journal*, 46(9):2081–2089.
- Mazmanyan, L., Ohanyan, V., and Treitsch, D. (2008). The Lognormal Central Limit Theorem for Positive Random Variables. *Working Paper*.
- Nunn, N. and Puga, D. (2012). Ruggedness: The Blessing of Bad Geography in Africa. *Review of Economics and Statistics*, 94(1):20–36.
- O'Rourke, S., Vu, V., and Wang, K. (2016). Eigenvectors of random matrices: A survey. *Journal of Combinatorial Theory, Series A*, 144:361–442.